MATHEMATICAL MODELING OF CANNABINOID RECEPTOR TYPE 2 ENDOCYTOSIS AND TRAFFICKING

by

Yan Zhang

BS, Nanjing University of Chinese Medicine, 2014

Submitted to the Graduate Faculty of

School of Pharmacy in partial fulfillment

of the requirements for the degree of Master of Science

University of Pittsburgh

2016

UNIVERSITY OF PITTSBURGH

SCHOOL OF PHARMACY

This thesis was presented

by

Yan Zhang

It was defended on

March 20, 2016

and approved by

Xiang-Qun Xie, PhD, MBA, Department of Pharmaceutical Sciences

LiRong Wang, PhD, Department of Pharmaceutical Sciences

Levent Kirisci, PhD, Department of Pharmaceutical Sciences

Thesis Advisor: Xiang-Qun Xie, PhD, MBA, Department of Pharmaceutical Sciences

MATHEMATICAL MODELING OF CANNABINOID RECEPTOR TYPE 2 ENDOCYTOSIS AND TRAFFICKING

Yan Zhang, BS

University of Pittsburgh, 2016

ABSTRACT

G-protein coupled receptor (GPCR) sensitization and desensitization, served as mechanisms to turn the system on and off in response to various ligands, involves mainly the endocytosis and trafficking of receptors. In this study, I utilized a mathematical model to investigate the endocytosis and trafficking of cannabinoid receptor type 2 (CB2), a GPCR highly expressed in the immune system. Two published experimental studies have provided some quantitative data demonstrating the time course of receptor phosphorylation, internalization, dephosphorylation, and recycling under various conditions in transfected Chinese Hamster Ovary cells. Based on these datasets, I developed an ordinary differential equation (ODE)-based model with the assumption that ligands regulate receptor endocytosis and trafficking only by affecting the activation of receptors on the cell surface. Fitting of this model to the data using Markov chain Monte Carlo (MCMC) method suggested that receptor constitutive trafficking is a fundamentally different process than the receptor trafficking under ligand treatment. The key difference between the two processes was shown to be the transfer of receptors from sorting endosome to recycling endosome, and the dephosphorylation of internalized receptors. The model was then modified according to this finding, and the subsequent fitting of the revised model showed a good accordance with the data.

Key words: Cannabinoid Receptor Type 2; Desensitization; Sensitization; ODE-based Model; Markov Chain Monte Carlo

TABLE OF CONTENTS

LIST OF FIGURES

1. INTRODUCTION

1.1 The Paradigm of G-protein Coupled Receptor Signaling

It is commonly believed that G-protein coupled receptor (GPCR) signaling begins with the binding of ligand to the extracellular region of the receptor, followed by a conformational change in the intracellular region which results in the activation of the either pre-coupled or encountered G-protein[1–3]. Simple as it seems, what truly happens in the cell can be far more complicated than such description. For many receptors in the GPCR family, including β_2-adrenoceptor and cannabinoid receptor type 2 (CB2), they exist in both active and inactive forms under an equilibrium between the two conformations even prior to ligand binding[4–6]. The difference in the intrinsic efficacy between agonist and inverse agonist thus can be explained by the fact that agonist stabilizes the active form of the receptor, while inverse agonist stabilizes the inactive form[3,6].

The receptor does not necessarily need to pre-couple to the G-protein before ligand binding. Free G-proteins randomly diffuse on the membrane, and are activated upon the collision with diffusing ligand-induced or spontaneously activated receptors[7]. Extensive evidences also have shown that in the presence of agonist, the receptor dynamically changes its conformation among different sub-states that could couple to not only G-proteins, but also G-protein coupled receptor kinase (GRK) or arrestins, inducing uncanonical downstream signaling events[8–11].

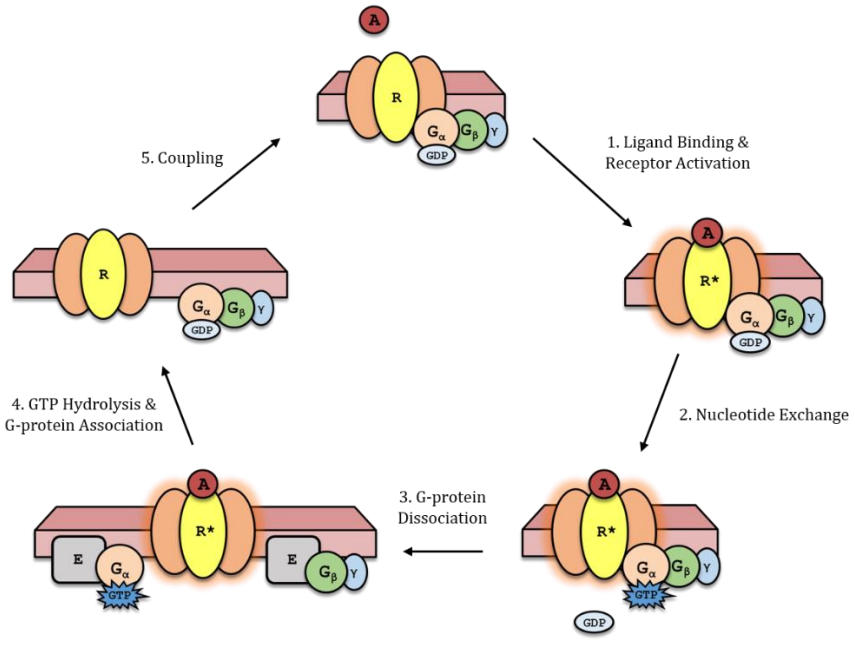

Figure 1. The early events of GPCR signaling. A: agonist; R: receptor.

The terminology "G-protein activation" covers several specific steps of reactions. G-protein is essentially a heterotrimer consisting of α, β, and γ subunits. When not activated, a GDP molecule binds to the Gα subunit. Once activated, a GTP molecule replaces GDP, and receptor-G-protein complex dissociates into an uncoupled receptor, a Gα-GTP subunit, and a Gβγ complex. Gα-GTP and Gβγ are able to interact with a variety of downstream effectors, depending on the specific type of the G-protein. The activation turns off when the bound GTP is hydrolyzed by the GTPase activity of Gα itself. Free Gα-GDP re-associates with Gβγ to form the inactive G-protein again, and thus far finishes a G-protein activation/inactivation cycle[7]. In an alternative theory, however, the α subunit of G_i-protein, named for its inhibitory effect on adenylyl cyclase, does not dissociate from Gβγ; instead, the heterotrimer experiences a subunit rearrangement upon activation, according to experimental observations[12]. The biological relevance of this finding is yet to be determined, but it has demonstrated that the interactions in GPCR system can be very diverse and complicated.

G-proteins can be classified into four categories mainly based on their α subunits: G_s, G_i, G_q, $G_{12/13}$. The α subunit of G_s-protein, upon activation, stimulates the activity of adenylyl cyclase, and hence leads to an increase in the second messenger cyclic AMP (cAMP)[13]. All β-adrenergic receptors couple to this type of G-protein, as well as other GPCRs like some serotonin (5-HT) receptors[14], Histamine H_2 receptor[15], Dopamine receptors D_1 and D_5[16], etc. The activated α subunit of G_i-protein, as opposed to G_s-protein, inhibits the adenylyl cyclase in the presence or absence of G_s α subunits[13]. CB receptors[17,18], Opioid δ, κ, μ receptors[19], Acetylcholine M_2 & M_4 receptors[20], and Chemokine CXCR4 receptor[21] are all G_i-protein coupled receptors. In addition, β_2-adrenergic receptor is also reported to be able to couple to G_i-protein after prolonged agonist treatment, supposedly through the action of PKA[22]. G_q-protein stimulates the production of two second messengers, inositol trisphosphate (IP_3) and diacylglycerol (DAG), by activating membrane-bound phospholipase C-β (PLC-β) that cleaves phosphatidylinositol 4,5-bisphosphate (PIP_2)[23]. Receptors coupled with G_q-protein includes 5-HT_2 receptor[14], α_1-adrenergic receptor[24], H_1 receptors[15], etc. $G_{12/13}$ are the latest found G-proteins among the four categories, shown to regulate actin cytoskeleton reorganization through interaction with guanine nucleotide exchange factors for Rho/Rac/Cdc42-like GTPases (RhoGEFs)[25].

1.2 CB2 Signaling, Endocytosis, and Trafficking

CB2 is coupled to G_i-protein, of which activated α subunit, as mentioned before, has an inhibitory effect on the downstream effector adenylyl cyclase, leading to a decrease in the cellular concentration of cAMP. Four cAMP molecules can symmetrically bind to two regulatory subunits of an inactive Protein Kinase A (PKA) complex, resulting in the release of two catalytic subunits with active catalytic site (activated PKA, or simply PKA when there is no confusion)[26]. Activated PKA is able to phosphorylate a broad range of proteins leading to either enhanced or inhibited activity. For example, cAMP response element-binding protein (CREB), a transcription factor binds to DNA sequences called cAMP response element (CRE) enhancing or reducing the transcriptional level of downstream genes[27]. CB2 is also reported to activate ERK-MAPK via PI_3K/Akt pathway that leads to cell migration[28], and induce calcium transients through PLC-β[29,30].

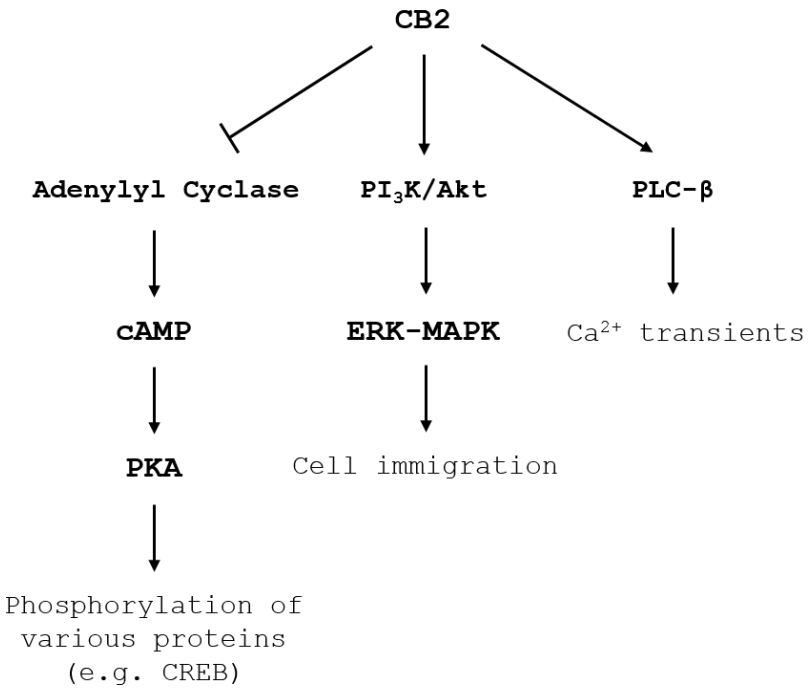

Figure 2. Diagram for known CB2-initiated signaling pathways.

PKA-phosphorylation is typically considered as a mean of desensitizing GPCR and shutting down prolonged signaling, especially for GPCRs which couple to Gs-protein, by precluding the receptor coupling to G-protein[31,32]. For Gi-protein coupled receptors, such as CB2, the desensitization theory seems however to be irrelevant as the inhibition of adenylyl cyclase will lead to a decrease in cAMP[33], which amounts to decreased PKA activation. Meanwhile, even if such interaction does exist, the mutual inhibition between CB2 and PKA will possibly lead to the bistability of the system, which is by no means a desensitization mechanism[34]. A study conducted

by Bouaboula et al. suggested that CB2 signaling pathway, including PKA activation, is not involved in the desensitization of CB2[35].

Another important kinase GRK, briefly mentioned above, is capable of phosphorylating many GPCRs including CB2, ensuing its decoupling from G-protein and endocytosis. The GRK-phosphorylated receptors bind to arrestin, which targets the receptor to clathrin-coated pits, where surface proteins are internalized[10,36]. Presumably GRK only phosphorylates activated receptors, and unlike PKA, its activation is mostly considered to be independent of activated Gα. It has been reported that the recruitment of GRK2 in β_2-adrenoceptor system involves released Gβγ[37], but as mentioned before, Bouaboula et al. demonstrated that in CB2 this is unlikely to be the case[35].

The receptors are internalized, mediated by Rab5, a monomeric G-protein that facilitates transportation of membrane proteins, and translocate to early endosomes, where the acidic pH stabilizes the receptors in a conformation that is a suitable substrate for phosphatase[38]. It is thus far unclear about which phosphatase catalyzes the dephosphorylation of CB2 receptor, but evidences indicate it might be a phosphatase-2A (PP2A) type phosphotase[35]. The dephosphorylated receptors are sorted either to degradation pathway, or alternatively to the recycling pathway, by which the receptors are transported back to the cell surface. Rab4-mediated fast recycling occurs with an estimated half-life in minutes (e.g. 5 min for transferrin receptor)[38], but the slow recycling of CB2 suggests it is likely to be through recycling endosome mediated by Rab11[39].

1.3 Kinetic Modeling as a Biological Research Method

The law of mass action, which depicts the rate of a chemical reaction to be proportional to the product of the concentrations of involved reactants to the power of order of reaction, has been extensively used in biochemistry for decades to study enzymatic reactions and physical contacts of proteins. The famous Michealis-Menten equation relating enzymatic reaction rate to the concentration of substrate and enzyme is derived from a series of ordinary differential equations (ODEs) given by the very law of mass action[40], and it turns out to be almost as equally useful in modeling complex biological systems as it is useful in the characterization of enzymatic reaction data. Today, mathematical models of biological systems using these kinetic laws are generally called kinetic models[41]. Because of the ability to generate time-dependent data, kinetic models are particularly suitable for analyzing the dynamic behavior of a given biological system, including

hypersensitivity[42], bistability[34,43,44], negative feedback loop[45], etc. When necessary, the static behavior of a system can also be easily acquired by a steady state analysis of such models[46]. Mass action or Michealis-Menten kinetics only describes the temporal behavior of a particular component, hypothesizing the reaction to happen under a well-mixing condition[47]. With the advance of bio-imaging techniques, information regarding the spatiotemporal dynamics of many biological systems comes into sight. The traditional way, and perhaps the simplest way, to incorporate spatial factors is to divide the volume where reactions take place into compartments. Components are assigned to each compartment with their concentrations calculated using the volume of that compartment rather than the whole space; reactions other than transportations happened in different compartments are treated independently using kinetic laws[48,49]. Another popular way of modeling spatiotemporal dynamics is using partial differential equations (PDEs), where the quantity of a component is a function of time and coordinates of the space. In PDE-based models, temporal relationship is still mostly governed by law of mass action, whereas the spatial relationship is depicted in terms of diffusion[50,51].

Kinetic modeling has proven to be valuable in studying biological phenomena[52–54]. In the area of drug design and development, such modeling style has pervaded every aspect of pharmacokinetics (PK) and pharmacodynamics (PD). One good example would be mechanistic PK/PD models, which is built to understand the metabolism (PK aspect) and action (PD aspect) of a drug, and further to predict the optimal dose or dosage regimen for clinical trials[55,56]. In analytical pharmacology, kinetic modeling is extensively utilized to understand the interaction between drug molecules and biological targets (e.g. receptors, enzymes, DNAs, etc.), and to predict possible outcomes resulted from certain pharmacological manipulations[57,58]. Although promising, kinetic modeling is never almighty, and challenges have yet to be overcome. The stochastic simulation of large scale kinetic models could be slow, particularly when both fast and slow reactions are present[59,60]. Numerical values for kinetic constants or other parameters are prerequisites, which is rather tricky to obtain in the context of biology. Biochemical reactions typically are coupled to one another, forming a complicated network with almost everything involved, making it difficult to decide which components should be included in the model and which should not. These limitations entail that we can only model and make predictions for biological systems that is allowed to be observed by any means. Model is not a replacement for experiment; rather it is a complementary tool to experimental methods that together facilitate our understanding of nature.

1.4 Previous Relevant Kinetic Models

1.4.1 Clark's Model: Ligand-Receptor Interaction

In 1933, Clark proposed a classical equilibrium model for ligand-receptor binding, where the interaction between ligand (L) and receptor (R) is simply modelled as a reversible reaction[61]:

$$\mathrm{L} + \mathrm{R} \underset{k_-}{\overset{k_+}{\rightleftharpoons}} \mathrm{LR}$$

In the light of law of mass action, the rate of the production of LR can be written as:

$$\frac{\mathrm{d}[\mathrm{LR}]}{\mathrm{d}t} = k_+[\mathrm{L}][\mathrm{R}] - k_-[\mathrm{LR}] \tag{1.4.1}$$

Assuming that initially the quantity of R is R0 and that of LR is 0. The number of receptors are conserved within the duration of reaction, so we have:

$$[\mathrm{R}] + [\mathrm{LR}] = R_0 \tag{1.4.2}$$

In most cases ligand molecules bound to the receptors only occupy a relatively small portion of the total, so it is safe to assume that [L] does not vary with the time, being only a constant in the equation. The solution of Eq.1.4.1 thus can be obtained and is as follows:

$$[\mathrm{LR}]_t = \frac{k_+[\mathrm{L}]R_0}{k_+[\mathrm{L}] + k_-}\left(1 - e^{-(k_+[\mathrm{L}]+k_-)t}\right) \tag{1.4.3}$$

Under the constraint Eq.1.4.2, the analytical form of [R] as a function of time is simply:

$$[\mathrm{R}]_t = R_0\left(1 - \frac{k_+[\mathrm{L}]R_0}{k_+[\mathrm{L}] + k_-}\left(1 - e^{-(k_+[\mathrm{L}]+k_-)t}\right)\right) \tag{1.4.4}$$

Thus far we have obtained the closed-form expressions for all the components, namely R and LR, in the model, as functions of time. In most scenarios, however, we are mainly interested in the steady state of the model, for drug actions after reaching equilibrium predominately produce the therapeutic outcome. In the sense of mathematics, we are interested in the limits:

$$[\mathrm{LR}]_\infty = \frac{k_+[\mathrm{L}]R_0}{k_+[\mathrm{L}] + k_-} \tag{1.4.5}$$

$$[\mathrm{R}]_\infty = \frac{k_-R_0}{k_+[\mathrm{L}] + k_-} \tag{1.4.6}$$

From Eq.1.4.5 and Eq.1.4.6, we can get:

$$\frac{[\mathrm{LR}]_\infty}{[\mathrm{L}][\mathrm{R}]_\infty} = \frac{k_+}{k_-} \tag{1.4.7}$$

The right hand side of Eq.1.4.7 is no more than a constant. Customarily we define the association constant K_a to be:

$$K_a \stackrel{\text{def}}{=} \frac{k_+}{k_-} \tag{1.4.8}$$

Whence,

$$\frac{[\mathrm{LR}]_\infty}{[\mathrm{L}][\mathrm{R}]_\infty} = K_a \tag{1.4.9}$$

Eq.1.4.9 is essentially the chemical equilibrium equation, in which the infinity symbols are removed for simplicity. It is obvious that with a higher association constant K_a, more L and R will associate to yield LR complex, which amounts to a higher affinity of drug molecule for the receptor.

The reciprocal of K_a, dissociation constant K_D, is also a measure of affinity and will be used later on. Define drug response E to be the fraction of ligand-occupied receptors:

$$E \stackrel{\text{def}}{=} \frac{[\mathrm{LR}]}{R_0} \tag{1.4.10}$$

With Eq.1.4.2, Eq.1.4.9, and simple algebra:

$$E = \frac{[\mathrm{L}]}{[\mathrm{L}] + K_D} \tag{1.4.11}$$

The plot of this function against log[L] is a sigmoidal curve, resembling the dose-response curve commonly seen in pharmaceutical sciences. To account for drugs with similar affinity but different efficacy, the model is modified by introducing a coefficient κ, ranging from 0 to 1[62]:

$$E = \frac{\kappa\,[\mathrm{L}]}{[\mathrm{L}] + K_D} \tag{1.4.12}$$

1.4.2 Emax Model

Noting that in Eq.1.4.12, when $[\mathrm{L}] \to \infty$, the response would reach its maximum. At the same point, we will have $[\mathrm{L}] >> K_D$, therefore:

$$E_{max} = \kappa \tag{1.4.13}$$

Denote the quantity of ligand when half of maximum response is reached as ED_{50}, with Eq.1.4.13 considered, then:

$$\frac{1}{2}\kappa = \frac{\kappa\, \mathrm{ED}_{50}}{\mathrm{ED}_{50} + K_D} \tag{1.4.14}$$

Whence,

$$\mathrm{ED}_{50} = K_D \tag{1.4.15}$$

To account for baseline response, a constant E0 shifting the curve along the y-axis is introduced. So finally we have:

$$E = E_0 + \frac{E_{max}[\mathrm{L}]}{\mathrm{ED}_{50} + [\mathrm{L}]} \tag{1.4.16}$$

Sometimes when the receptor is capable of accepting multiple ligands simultaneously, a Hill coefficient *n* is present in Eq.1.4.16 to reflect binding cooperativity[63]:

$$E = E_0 + \frac{E_{max}[\mathrm{L}]^n}{\mathrm{ED}_{50}{}^n + [\mathrm{L}]^n} \tag{1.4.17}$$

In which an *n* greater than 1 means positive cooperativity, an *n* less than 1 means negative cooperativity, and an *n* of unity amounts to independent binding. For the shape of the curve, a large *n* leads to a steep slope of the log-linear region, as shown in Figure 3.

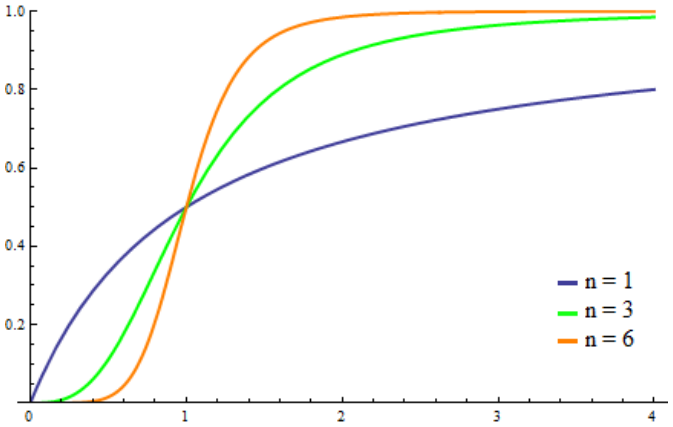

Figure 3. Hill function plotted with different *n*.

1.4.3 Ternary Complex Model

Clearly, drug action does not stop at binding; the binding between the drug molecule and the receptor is just a beginning of a series downstream signaling events. Biological transducers,

such as G-proteins, serve not only as messengers but also adjustable elements in the pathway, so it is crucial to incorporate their presence in the mathematical model. The Ternary Complex Model (TCM) is proposed for above reasons, with a simple extension of the coupling of receptor to G-protein[64]:

$$\begin{aligned} \mathrm{L} + \mathrm{R} &\rightleftharpoons \mathrm{LR} \\ \mathrm{LR} + \mathrm{G} &\rightleftharpoons \mathrm{LRG} \end{aligned}$$

There is no closed-form solution for ODEs depicting these two reactions; actually such and more complicated systems are typically solved numerically using computers. But it is still possible to solve them for steady state solution, by noting that under multiple equilibria:

$$K_a = \frac{[\mathrm{LR}]}{[\mathrm{L}][\mathrm{R}]} \tag{1.4.18}$$

$$K_g = \frac{[\mathrm{LRG}]}{[\mathrm{LR}][\mathrm{G}]} \tag{1.4.19}$$

As well as the constraint:

$$[\mathrm{R}] + [\mathrm{LR}] + [\mathrm{LRG}] = R_0 \tag{1.4.20}$$

The response E can be derived:

$$E \stackrel{\text{def}}{=} \frac{[\mathrm{LRG}]}{R_0} = \frac{K_g K_a [\mathrm{G}][\mathrm{L}]}{1 + K_a[\mathrm{L}] + K_g K_a [\mathrm{G}][\mathrm{L}]} \tag{1.4.21}$$

Compared to Eq.1.4.11 and Eq.1.4.12, we can clearly see how coupling of receptor to G-protein contributes to the response: in the numerator, a factor of $K_g[\mathrm{G}]$ is added in Eq.1.4.21, corresponding to κ in Eq.1.4.12; in the denominator, an additional term with the same form of the numerator is added. It is then reasonable to postulate that in addition to binding affinity, drug molecules can affect the response by either facilitating or hampering receptor coupling to G-protein, which is probably achieved by inducing different conformations of LR complexes.

This explanation on intrinsic efficacy of GPCR drug, although rudimentary, turns out to be correct in some sense, and it is in effect a good example of how mathematical modelling can help us understand the way by which biological systems work.

1.4.4 Two-State Ternary Complex Model

Proteins are not static rigid bodies; rather, they are dynamic elastic objects which fluctuate among various states. As mentioned in section 1.1, substantial evidences have shown that GPCRs can switch back and forth, either spontaneously or induced by ligand-binding, between an active state and an inactive state. To model this observation, the extended Ternary Complex Model (eTCM) is proposed[65]:

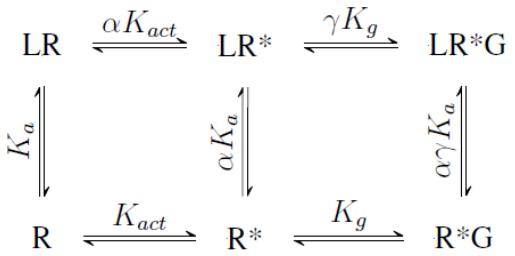

In which R* stands for the active form of the receptor, and only equilibrium constants are shown in the scheme. Because all the reactions in the system are reversible reactions, detailed balance implies that, between any pair of nodes (e.g. R and LR*), no matter which route you take to travel from one to another, the product of equilibrium constants are the same. This gives us an interesting insight that if a ligand promotes receptor activation (most likely an agonist), then it would also prefer binding to the active form of the receptor rather than the inactive form, which implies the same logics mentioned in Section 1.1, that the agonist stabilizes the active form while the inverse agonist stabilizes the inactive form.

Using similar technique in Section 1.4.1, and noting that only LR*G and R*G give rise to downstream signaling, the response can thus be written as follows:

$$E = \frac{K_{act}K_g[\mathrm{G}](1+\alpha\gamma K_a[\mathrm{L}])}{1+K_{act}+K_a[\mathrm{L}](1+\alpha K_a)+K_{act}K_g[\mathrm{G}](1+\alpha\gamma K_a[\mathrm{L}])} \tag{1.4.22}$$

Particularly, when ligand is absent, the system still possesses a basal level of response:

$$E_0 = \frac{K_{act}K_g[\mathrm{G}]}{1+K_{act}+K_{act}K_g[\mathrm{G}]} \tag{1.4.23}$$

Which is the so-called *constitutive activity* of GPCR systems, mentioned briefly in Section 1.1 from a biological perspective. As we can see, the level of constitutive activity, or basal response E_0, depends on receptor activation equilibrium constant K_{act}, coupling equilibrium constant K_g, and the quantity of free G-protein. Rearrange Eq.1.4.23 by dividing the numerator into both sides of the fraction line:

$$E_0 = 1/\left(\frac{1}{K_{act}K_g[\mathrm{G}]} + \frac{1}{K_g[\mathrm{G}]} + 1\right) \tag{1.4.24}$$

Apparently when [G] does not vary, larger K_{act} and K_g lead to higher E_0. However [G] is in fact a function of K_{act} and K_g, as higher receptor activation and coupling equilibrium constants amount to more G-protein binding to the receptor, but considering that (a) the level of spontaneous receptor activation is low ($K_{act} \approx 0.1 \sim 0.01$[66]), and (b) receptors are outnumbered by G-proteins under normal conditions, the above analysis generally holds true.

It is quite difficult to understand how α and γ decide the effect of a ligand on the system from Eq.1.4.22, so instead we consider that when [L] $\rightarrow \infty$, the response reaches its maximum:

$$E_{max} = \frac{\alpha\gamma K_{act}K_g[\mathrm{G}]}{1 + \alpha K_{act} + \alpha\gamma K_{act}K_g[\mathrm{G}]} \tag{1.4.25}$$

To compare with basal response E_0, we take the ratio of Eq.1.4.25 and Eq.1.4.23:

$$\frac{E_{max}}{E_0} = \frac{\alpha\gamma + \alpha\gamma K_{act} + \alpha\gamma K_{act}K_g[\mathrm{G}]}{1 + \alpha K_{act} + \alpha\gamma K_{act}K_g[\mathrm{G}]} \tag{1.4.26}$$

The necessary and sufficient condition of $E_{max} > E_0$ is that the numerator of the right hand side of Eq.1.4.26 is greater than the denominator, which amounts to:

$$\alpha\gamma - 1 + \alpha K_{act}(\gamma - 1) > 0 \tag{1.4.27}$$

Suppose that the ligand binding does not affect G-protein coupling ($\gamma = 1$), Eq.1.4.27 reduces to:

$$\alpha > 1 \tag{1.4.28}$$

In such circumstance, therefore, if a ligand is able to facilitate receptor activation or has higher affinity for active receptors ($\alpha > 1$), the ligand is an agonist. Conversely if a ligand hampers receptor activation or has higher affinity for inactive receptors ($\alpha < 1$), the ligand is an inverse agonist. When the ligand has no effect on receptor activation and has equal binding affinity for active and inactive receptors, the ligand will compete with other ligands for the binding site on receptors, thus being a neutral antagonist.

If the ligand binding can affect G-protein coupling – which is very likely according to recent findings that GPCRs possess more than one active conformation and can be induced by different ligands, causing ligand-biased downstream signaling – different combinations of α and γ can lead to either agonism or inverse agonism[9,11]. It suffices to show that, however, if both α and

γ are greater than one, the ligand is agonist; if both α and γ are less than one, the ligand is inverse agonist.

Inspired by the idea that receptor and G-protein can be coupled without receptor activation, a more comprehensive model – cubic Ternary Complex Model (cTCM) is proposed[67]:

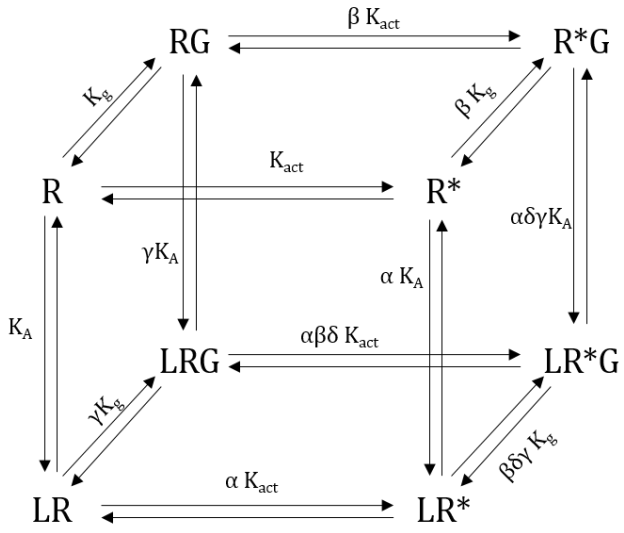

Figure 4. The cubic Ternary Complex Model.

The cTCM can be analyzed under steady state with aforementioned methods as well, and the implications of the model can be found in many literatures[3,67–69]. An additional parameter controls the effects of ligand in cTCM, which is a factor that indicates the interactions among ligand-binding, G-protein coupling, and receptor activation, making the response of the model even more complex. Nevertheless, the conclusions on α, γ, and agonism/inverse agonism still apply.

1.4.5 Other Relevant Models

(1) A kinetic model of GRK-mediated β_2-adrenoceptor regulation[70].
(2) A kinetic model for VEGFR2 signaling and trafficking[71].
(3) A kinetic model for CXCR4 and CXCR7 competition for β-arrestin and trafficking[72].
(4) A compartmental model of β_1 and M_1 receptor systems in cardiac myocyte, which includes caveolar, extra-caveolar, and cytoplasmic compartments[49].

The list is not an exhaustive one, but all of which are pertinent to the study of this thesis.

2. METHODS AND MATERIALS

2.1 Experimental Datasets

A total of six datasets from two published studies are used in this study to develop the model and estimate parameters. Two datasets from Bouaboula et al. for the time course of unphosphorylated CB2 receptor concentration in response to agonist (30 nM CP-55940) or inverse agonist (50 nM SR 144528) treatment, called as "phosphorylation data" in this thesis, are used for estimating the phosphorylation and dephosphorylation rate constants[35]. The original data is an immunoblotting of CB2 receptor with an antibody, which is converted into percentage changes for data fitting, using software ImageJ, in this study. There is only one single experiment so there is no error bar in the data.

The other four datasets are from Grimsey et al.'s work[39]. Two of the datasets are under constitutive condition, called as "constitutive data" in this thesis, where surface receptors are labeled with a primary antibody, then allowed to internalize constitutively, and finally detected using a secondary antibody. Two conditions are used for secondary antibody binding: (a) under permeabilizing condition, the secondary can penetrate the cell membrane and hence detect all primary antibody-labeled receptors, so data obtained under this condition demonstrate the constitutive degradation of CB2 receptors; (b) under non-permeabilizing condition, the secondary antibody cannot enter into the cell, and therefore is only able to bind to surface primary antibody-labeled receptors. Data obtained under this condition demonstrate the constitutive internalization of CB2 receptors. The other two datasets show the percentage change in number of surface receptors in response to agonist (1μM HU-308) or inverse agonist (1μM AM630) treatment, which is called as "ligand treatment data" in this thesis. All of these four datasets are acquired from three independent experiments, so an error bar is present in each of these datasets.

2.2 ODE-Based Model for CB2 Endocytosis and Trafficking

The model describes the biochemical reactions in terms of law of mass action (LMA), which for a single reaction states as[47]:

$$\frac{\mathrm{d}P}{\mathrm{d}t} = k \prod_i {S_i}^{\nu_i}$$

Where P stands for product, t stands for time, k stands for the rate constant, S_i stands for the i-th substrate, and v_i stands for the order of reaction for S_i. For coupled reactions, the total rate for the production or depletion of a particular species is simply the summation of the rates for all individual reactions. In particular for the CB2 endocytosis and trafficking system that I am interested in, the structure of the system is shown as follows:

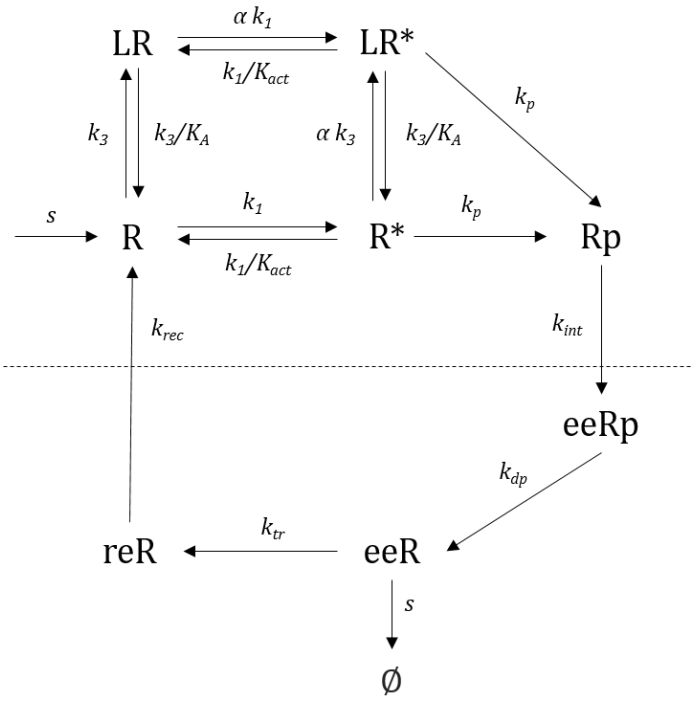

Figure 5. The structure of the kinetic model. R: inactive receptor; R*: active receptor; LR, LR*: ligand-bound receptor; Rp: phosphorylated receptor; eeR, eeRp: receptor in early endosome; reR: receptor in recycling endosome.

Where the letters indicate species (or biological entities), the arrows indicate reactions, and letters in italics above each arrow represents the rate constant for that particular reaction. Species are divided into two compartments generally in this model. As shown in Figure 5, above the dash line is the cell surface, and below the dash line is the endosome compartment. Mass transportation between the two compartments manifests as the internalization reaction, of which rate constant is k_{int}, and the recycling reaction, of which rate constant is k_{rec}. Reactions take place on two time scales: the interaction between receptor and ligands, as well as the activation of receptor, which is much faster than the receptor trafficking processes. Mathematically, all the coupled reactions as a whole, compose a system of ODEs describing the temporal dynamics for each species:

$$\dot{R} = -k_1 R + \frac{k_1}{K_{act}} R^* - k_3 L \cdot R + \frac{k_3}{K_a} LR + k_{rec} reR + s \tag{2.2.1}$$

$$\dot{R^*} = k_1 R - \frac{k_1}{K_{act}} R^* - \alpha k_3 L \cdot R^* + \frac{k_3}{K_a} LR^* - k_p R^* \tag{2.2.2}$$

$$\dot{LR} = -\alpha k_1 LR + \frac{k_1}{K_{act}} LR^* + k_3 L \cdot R - \frac{k_3}{K_a} LR \tag{2.2.3}$$

$$\dot{LR^*} = \alpha k_1 LR - \frac{k_1}{K_{act}} LR^* + \alpha k_3 L \cdot R^* - \frac{k_3}{K_a} LR^* - k_p LR^* \tag{2.2.4}$$

$$\dot{R_p} = k_p R^* - k_{int} R_p \tag{2.2.5}$$

$$\dot{eeR_p} = k_{int} R_p - k_{dp} eeR_p \tag{2.2.6}$$

$$\dot{eeR} = k_{dp} eeR_p - k_{tr} eeR - s \tag{2.2.7}$$

$$\dot{reR} = k_{tr} eeR - k_{rec} reR \tag{2.2.8}$$

Note that the degradation of receptors is modeled as a zero-order reaction with a rate of *s*, to account for the experimental observation that agonist treatment does not increase degradation[39,73], which contradicts the behavior of a first-order process whose rate is linearly dependent of the number of internalized receptors increased as a result of agonist stimulation. Ligand concentration is assumed to be a constant that is independent of the reactions. The total number of receptors remains unchanged throughout the experiment, therefore a zero-order rate of synthesis is used to account for this observation. Since both synthesis and degradation are zero-order reactions, so the following initial condition is vital for both simulation and analytical solution:

$$R_0 = R + R^* + R_p + eeR_p + eeR + reR \tag{2.2.9}$$

There is no term for ligand-bound receptors in Eq.2.2.9 because in most experimental procedures, cells have already reached the steady state before any ligand addition.

2.3 Solving the Constitutive Steady State Analytically

The term "constitutive steady state" means (a) constitutive: before ligand treatment; (b) steady state: the concentrations of all the species in the system do not vary with time (or fluctuate within a very small region due to various noise source). Solving the ODEs analytically for this state is desirable for numerical simulations because it spares the trouble of simulating the system to reach constitutive steady state before ligand addition, of which time scale is hard to determine

and can be time-consuming when being run for thousands of times for parameter estimation or sensitivity analysis. The system of ODEs for the case where no ligand is present can be reduced to six ODEs where the concentrations for ligand-bound species are 0, and written in the matrix form:

$$\begin{bmatrix} \dot{R} \\ R^* \\ R_p \\ eeR_p \\ eeR \\ reR \end{bmatrix} = \begin{bmatrix} -k_1 & \frac{k_1}{K_{act}} & 0 & 0 & 0 & k_{rec} \\ k_1 & -\frac{k_1}{K_{act}} - k_p & 0 & 0 & 0 & 0 \\ 0 & k_p & -k_{int} & 0 & 0 & 0 \\ 0 & 0 & k_{int} & -k_{dp} & 0 & 0 \\ 0 & 0 & 0 & k_{dp} & -k_{tr} & 0 \\ 0 & 0 & 0 & 0 & k_{tr} & -k_{rec} \end{bmatrix} \begin{bmatrix} R \\ R^* \\ R_p \\ eeR_p \\ eeR \\ reR \end{bmatrix} + \begin{bmatrix} s \\ 0 \\ 0 \\ -s \\ 0 \end{bmatrix} \quad (2.3.1)$$

Denote the species variable vector as $\vec{r}$, the first-order reaction rate constant matrix as $\boldsymbol{A}$, and the zero-order reaction rate constant vector as $\vec{b}$, then Eq.2.3.1 can be written as:

$$\dot{\vec{r}} = \boldsymbol{A}\,\vec{r} + \vec{b} \quad (2.3.2)$$

At steady state, the rates are all zero:

$$\vec{0} = \boldsymbol{A}\,\vec{r} + \vec{b} \quad (2.3.3)$$

Together with the initial condition Eq.2.2.9, the steady solution can be solved analytically, which is done using Wolfram Mathematica 9.0 in this study.

2.4 Numerical Simulation of The System

With the initial condition for constitutive steady state determined analytically in last section, the concentration of each species as a function of time under ligand treatment can be solved numerically using an ODE solver. In general, the numerical solver takes an extremely small time step Δt, and iteratively calculates the value for variable x based on the approximation[74]:

$$\Delta x = f(x, t)\,\Delta t \quad (2.4.1)$$

Here, $f(x, t)$ is the function for reaction rates determined by LMA. Advanced numerical solvers typically choose Δt adaptively to satisfy certain tolerance for error, and improve integration accuracy using Runge-Kutta methods[75]. In this study, ODEs are solved numerically using ode15s solver in MATLAB, which is able to solve stiff ODEs rather quickly.

In particular, for simulations of the constitutive data, as introduced in Section 2.1, it should be noted that only *labeled species* can be read from data. A simple way to cope with this problem

is to simulate the dynamics of labeled species independently. For example, for the following toy model:

$$R \underset{k_2}{\overset{k_1}{\rightleftharpoons}} R^*$$

If we denote the number of labeled species with lowercase letters, *r* and *r**, and denote the total number with uppercase letters, *R* and *R**, we have:

$$\dot{r} = -k_1 R \frac{r}{R} + k_2 R^* \frac{r^*}{R^*} = -k_1 r + k_2 r^* \tag{2.4.2}$$

Where we consider that for a particular reaction, each molecule has an equal chance to be chosen to react, regardless of the labeling status, so the rate for labeled species is effectively the rate for total reaction times the probability that a labeled molecule gets chosen. In the end, we see that for linear systems the dynamics for labeled species is simply an isolated system that is independent of unlabeled ones. With that, the simulation procedure for labeled species is as follows:

(a) Calculate the initial condition analytically;
(b) Set concentrations for intracellular species to 0, mimicking the labeling procedure using primary antibodies;
(c) Simulate the system within a time duration of interest.

Zero-order degradation can lead to unrealistic situations where the concentration for the degrading species becomes negative, as shown in Figure 6 (A). Also zero-order kinetics is less capable of capturing delayed effect. Therefore, a piecewise function is used for degradation in simulation to circumvent these problems:

$$\frac{dX}{dt} = \begin{cases} -s, & when\ X > c \\ -\frac{s}{c} X, & when\ X \leq c \end{cases} \tag{2.4.3}$$

So that the degradation is first-order when the number of *X* is below the threshold *c*, and is zero-order otherwise, as shown in Figure 6 (B). In this study, the threshold *c* is set to 100 and it captures the delayed degradation for labeled species fairly well, which will be shown in Section 3, *Results*.

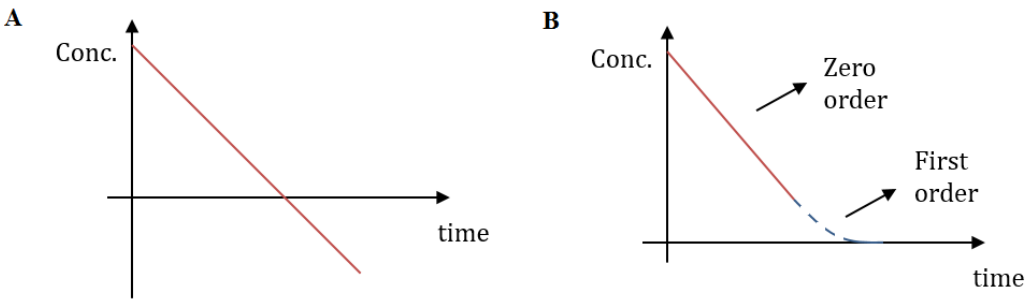

Figure 6. Schematic plots showing the time course of
(A) zero-order degradation, (B) a mixture of zero- and first-order degradation

2.5 Parameter Estimation Based on Literatures

The forward rate constant for ligand binding k_1, receptor activation k_3, and the binding affinity K_a for both agonist and inverse agonist are estimated based on values in other published experimental or computational works. Because in this study we are mainly interested in events occurring on the time scale of minutes or hours, so the k_1 and k_3 do not need to be very accurate and can be estimated coarsely based on general ligand binding rate and receptor activation rate constant for GPCRs. The ligand-receptor association constant K_a for agonist, HU-308 in this study is estimated based on a dose-response data published in Grimsey et al.'s work[39], and for inverse agonist, AM630, is determined by its EC50 in published binding assays[5,76].

The searching ranges for other parameters, which will be used for optimization algorithms as MCMC, are determined based on the values used in other computational studies. The total number of receptors is set to be 2500 – 50000, as determined by preliminary simulation of the system, as well as the number used in other published models[66,70].

2.6 Parameter Estimation Based on Optimization Algorithms

2.6.1 Nelder-Mead Algorithm

Nelder-Mead algorithm is a method to search for an optimal point in the parameter space that minimizes an arbitrarily defined loss function[77], which in my case is the sum of squares error between the experimental data and the simulated data. In the algorithm, a *simplex*, the convex hull of a set of $n+1$ linearly independent points defined in an n dimensional space, is placed in the parameter space initially, and then moved by changing the coordinates of its vertices using *Reflection*, *Expansion*, *Contraction*, or *Reduction* operators, through which the simplex tends to

move to positions where the loss function reaches a minimal value. It is a gradient-free method, for which it is suitable for minimizing functions with no closed form expression, but meanwhile it cannot guarantee a globally optimal solution[78], making it sensitive to the initial location of the simplex for functions with complicated landscape.

In this study the rate constants of GRK phosphorylation and dephosphorylation of receptor is estimated by fitting the following exponential function to a published experimental dataset using MATLAB built-in Nelder-Mead algorithm, *fminsearch*:

$$x(t; k, x_0, x_1) = (x_0 - x_1)e^{-kt} + x_1 \tag{2.6.1}$$

The Eq.2.6.1 is an exponential decay in either decreasing or increasing form, starting from x_0 and converging to x_1, and the rate constant k characterizes the time scale of the process and can be used as a starting point for further parameter estimation. The loss function is defined as follows:

$$f(\boldsymbol{\theta}) = \sum_i (x(t_i; \boldsymbol{\theta}) - y_i)^2 \tag{2.6.2}$$

Where $\boldsymbol{\theta}$ is a vector of parameters, which in this case is (k, x_0, x_1), and t_i is the i-th time point corresponding to the time point for y_i, the i-th experimental data point.

Eq.2.6.1 is fitted to the agonist-induced phosphorylation data and an inverse agonist-induced dephosphorylation data mentioned in Section 2.1 is used for estimating phosphorylation and dephosphorylation rate constants, respectively.

2.6.2 Markov chain Monte Carlo: Metropolis-Hastings Algorithm

Parameter estimation/search algorithms as Nelder-Mead algorithm commonly assume that there is one "correct" parameter set of the model for fitting the data, whereas we all know that most biological experimental observations are the total or averaged effects contributed from hundreds to thousands of cells or different biological samples. Even within a single cell, background "noise" originated from various sources, such as the stochastic synthesis of proteins or heterogeneous distribution of molecules, can easily dismiss the relevance of such mindset. The error bar in the experimental data also means that all the solutions are possible, and statistically, it is just a matter of probabilities[79,80].

MCMC is a family of techniques that can be used for parameter estimation in a statistically relevant way, and very different from parameter searching algorithms that aims for an "optimal

solution", it tries to map the probability distribution on the parameter space, given the known data $\boldsymbol{D}$, namely, the algorithm samples points in the parameter space according to $P(\boldsymbol{\theta}|\boldsymbol{D})$. What we get out of such algorithms, is a cluster of parameter sets that contribute to the fitting with certain likelihood, but in the meantime, we still have the option to pick out the optimal one with the largest likelihood and see if a single parameter set is good enough to fit the data.

Computing the posterior probability $P(\boldsymbol{\theta}|\boldsymbol{D})$ analytically, however, is difficult for most models. The trick is by applying the Bayes' rule:

$$P(\boldsymbol{\theta}|\boldsymbol{D}) = \frac{P(\boldsymbol{D}|\boldsymbol{\theta})P(\boldsymbol{\theta})}{P(\boldsymbol{D})} = \frac{P(\boldsymbol{D}|\boldsymbol{\theta})P(\boldsymbol{\theta})}{\int P(\boldsymbol{D}|\boldsymbol{\theta})P(\boldsymbol{\theta})\,\mathrm{d}\boldsymbol{\theta}} \tag{2.6.3}$$

Typically we do not care much about $P(\boldsymbol{D})$ since it is independent of $\boldsymbol{\theta}$ and basically serves as a normalization factor, so Eq.2.6.3 implies that we only need the likelihood $P(\boldsymbol{D}|\boldsymbol{\theta})$ and prior probability $P(\boldsymbol{\theta})$ to calculate the posterior:

$$P(\boldsymbol{\theta}|\boldsymbol{D}) \propto P(\boldsymbol{D}|\boldsymbol{\theta})\, P(\boldsymbol{\theta}) \tag{2.6.4}$$

The prior $P(\boldsymbol{\theta})$ is often set to be a uniform distribution on a given parameter. It is of course crucial to consider using a non-uniform prior probability distribution if a strong correlation between two or more parameters is found, but in this study, a uniform distribution is good enough for all parameters. The likelihood $P(\boldsymbol{D}|\boldsymbol{\theta})$ is often defined in the following form assuming a normally distributed noise in the data:

$$P(\boldsymbol{D}|\boldsymbol{\theta}) = \prod_i \frac{1}{\sqrt{2\pi}\sigma_i} \exp\left[-\frac{\left(y_i - x(t_i;\boldsymbol{\theta})\right)^2}{2{\sigma_i}^2}\right] \tag{2.6.5}$$

Where σ_i stands for the standard deviation of the i-th data point.

To sample random points from the now defined $P(\boldsymbol{\theta}|\boldsymbol{D})$ can be accomplished by using the Metropolis-Hastings algorithm, which uses a *random walker* that, in each iteration, attempts to visit a randomly chosen adjacent point in the parameter space, and this attempt gets either accepted or rejected based on a transition probability defined based on the posterior $P(\boldsymbol{\theta}|\boldsymbol{D})$ at the destination and that at the original point[81,82]. This is where the *Markov chain* in its name comes from, because each point in the parameter space can be seen as a state (or a node) in a Markov chain, and the transition probabilities between each pair of states are well-defined. It can be shown

that, for a random walker at $\boldsymbol{\theta}$ and a destination at $\boldsymbol{\theta}'$, it guarantees a unique equilibrium distribution for a Markov chain, when the acceptance criterion is:

$$P(\boldsymbol{\theta} \to \boldsymbol{\theta}') = \begin{cases} \dfrac{P(\boldsymbol{\theta}'|\boldsymbol{D})}{P(\boldsymbol{\theta}|\boldsymbol{D})}, & if\ P(\boldsymbol{\theta}'|\boldsymbol{D}) < P(\boldsymbol{\theta}|\boldsymbol{D}) \\ 1, & otherwise \end{cases} \tag{2.6.6}$$

From Eq.2.6.4 and Eq.2.6.5, and the fact that we choose uniform distribution as the priors $P(\boldsymbol{\theta})$, the ratio of posteriors can be easily calculated:

$$\frac{P(\boldsymbol{\theta}'|\boldsymbol{D})}{P(\boldsymbol{\theta}|\boldsymbol{D})} = \frac{P(\boldsymbol{D}|\boldsymbol{\theta}')}{P(\boldsymbol{D}|\boldsymbol{\theta})} = \frac{\prod_i \frac{1}{\sqrt{2\pi}\sigma_i} \exp\left[-\frac{\left(y_i - x(t_i;\boldsymbol{\theta}')\right)^2}{2{\sigma_i}^2}\right]}{\prod_i \frac{1}{\sqrt{2\pi}\sigma_i} \exp\left[-\frac{\left(y_i - x(t_i;\boldsymbol{\theta})\right)^2}{2{\sigma_i}^2}\right]}$$

$$= \exp\left[-\sum_i \frac{\left(y_i - x(t_i;\boldsymbol{\theta}')\right)^2}{2{\sigma_i}^2} + \sum_i \frac{\left(y_i - x(t_i;\boldsymbol{\theta})\right)^2}{2{\sigma_i}^2}\right] \tag{2.6.7}$$

The walking of the random walker is typically done by applying a small perturbation at its current location. As simple as it may sound, this perturbation procedure is, in practice, rather critical for the sampling efficient as well as the speed of convergence for the algorithm. First of all, for parameters that vary on the logarithm scale, the perturbation should be the *multiplication* of a uniformly sampled random number instead of an *addition*. Second, the magnitude of the perturbation should be adjusted for each parameters in terms of the range of variation to facilitate a faster convergence. A simple and elegant way to implement this is to normalize the parameters based on their range. For normalized parameters, the size of a perturbation step decides also the sampling efficiency: small perturbation steps dig deeply within a local optimal, but have little chance to explore globally, and *vice versa*. A common practice to optimize the sampling efficiency is by looking at the *acceptance rate*, which is reported to be optimal within the range of 0.25-0.5[83].

There is no built-in MCMC method in MATLAB, so I wrote my own script to implement the algorithm. For this particular study, the implementation is as follows:

(a) Based on current parameter set, create separate parameter sets (with different ligand properties or concentration) for constitutive steady state, agonist treatment, and inverse agonist treatment conditions, respectively.

(b) Simulate for the experimental data with labeled species as mentioned in Section 2.4, and calculate the likelihood.

(c) Simulate for the agonist treatment data, and calculate the likelihood.

(d) Simulate for the inverse agonist treatment data, and calculate the likelihood.

(e) Use the product of all the aforesaid likelihoods to determine if the current parameter set should be accepted or rejected based on the acceptance criterion Eq.2.5.6.

(f) If accepted, output current parameters as well as the corresponding likelihood.

(g) Perturb the parameters based on their range and scale.

Repeat (a)-(g) until convergence.

2.6.3 Latin Hypercube Sampling

Even though techniques like MCMC have the potential to escape a local optimal and thus be able to explore the whole parameter space, a trade-off for its ability to sufficiently sample the local geometry must be made. To reach both goals, a simple strategy is to generate multiple Markov chains whose initial points are widely spread over the parameter space, and naively, if we subdivide each parameter range into n bins, for an m-dimensional parameter space we can generate $m \times n$ Markov chains to make sure of a representative coverage of the whole space. This is usually unnecessary and impractical due to the large number of Markov chains which increases exponentially with the number of parameters m.

Alternatively, we can select initial points in the parameter space randomly from a uniform distribution, which is reasonable, as we assumed a uniform distribution for the prior probability $P(\boldsymbol{\theta})$. This method, however, suffers from the problem that, because of the relatively small number of initial points needed, it is difficult to guarantee that the randomly chosen initial points have a good coverage of the whole space. A better way to generate random initial points is through Latin Hypercube Sampling (LHS), a technique that can sufficiently generate n random points from the m-dimensional parameter space (if each dimension is subdivided into n bins), and meanwhile guarantee the coverage of the parameter space. The number of Latin Hypercube Sampled points is only dependent of the number of bins n into which each dimension is subdivided[84]. Take a 2-dimensional space as an example, a LHS point satisfy the criterion that it does not occupy the same column and row with any other point, as demonstrated in Figure 7:

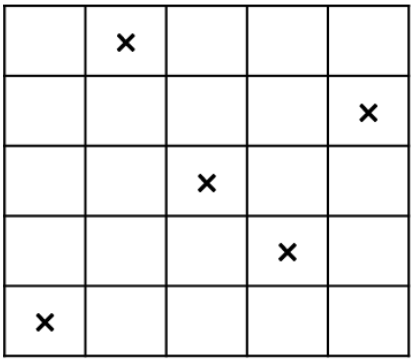

Figure 7. An example of LHS points in a 2D space subdivided into 5 bins for each dimension.

This technique is used in this study to generate initial points for the MCMC algorithm. For the 12 dimensional parameter space, typically 20-50 initial points are generated for each Markov chain to guarantee a sufficient sampling of the space.

2.6.4 Indicators for Goodness-of-Fit

It should be noted that the goal of this study is not to propose a regression model that aims to fit all experimental data for CB2 endocytosis and trafficking. The mechanistic model developed in this study tries to explain known experimental observations, and further offer new insights for understanding the mechanism of GPCR desensitization and resensitization. Data fitting techniques used in this study serve as means to bridge biological data and the theoretical model, to help understand how each parameter in the model plays a role in interpreting the data.

However, goodness-of-fit metrics are still needed and as indicators for "good fitting" and "poor fitting". Sum of squared error of prediction (SSE) is used in this study as a primary indicator for the discrepancy between data and the model, which is defined as[85]:

$$SSE = \sum_{i=1}^{l} (y_i - \hat{y}_i)^2 \tag{2.6.8}$$

Where l is the total number of data points, and for each data point y_i, there is a predicted value from the model $\hat{y}_i$. Because we do not have the original data points y_i's, and only have the mean and standard deviation for each time point, so we cannot use Eq.2.6.8 to calculate the SSE. Alternatively, if we have m parallel experiments and n time points (a total of $m \times n$ data points), we can use:

$$SSE = (m-1)\sum_{i=1}^{n}{\sigma_i}^2 + m\sum_{i=1}^{n}{\overline{y_i}}^2 - m\sum_{i=1}^{n}\left(2\overline{y_i}\widehat{y_i} - {\widehat{y_i}}^2\right) \tag{2.6.9}$$

Where σ_i is the standard deviation, $\overline{y_i}$ is the mean, and $\widehat{y_i}$ is the model-predicted value for *i*-th time point.

The ODE model in this study has 8-12 independent parameters, and with more parameters introduced into the model, it is more likely lead to over-fitting. To compare fitting between models with different number of parameters, Bayesian information criterion (BIC) can be used as a metric for goodness-of-fit, which is defined as follows[85]:

$$BIC = -2 \cdot \ln L_m + k \cdot \ln n \tag{2.6.10}$$

Where L_m is the maximized value for likelihood $P(\boldsymbol{D}|\boldsymbol{\theta})$, *k* is the number of parameters, and *n* is the number of data points. Lm can be calculated as the likelihood with a particular set of parameter which maximizes it. From Eq.2.6.5 in Section 2.6.2, L_m can be written as:

$$\begin{aligned} L_m &= \prod_i \frac{1}{\sqrt{2\pi}\sigma_i}\exp\left[-\frac{(y_i-\widehat{y_i})^2}{2{\sigma_i}^2}\right] \\ &= \left(\prod_i \frac{1}{\sqrt{2\pi}\sigma_i}\right) \times \exp\left[-\sum_i \frac{(y_i-\widehat{y_i})^2}{2{\sigma_i}^2}\right] \end{aligned} \tag{2.6.11}$$

For the same reason as that for the calculation of SSE, we cannot calculate the exponential term in Eq.2.6.11 directly since it requires the original data points y_i's. An alternative to calculate it is:

$$\sum_i \frac{(y_i-\widehat{y_i})^2}{2{\sigma_i}^2} = \sum_{i=1}^{n} \frac{(m-1){\sigma_i}^2 + m{\overline{y_i}}^2 - 2m\widehat{y_i}\overline{y_i} + m{\widehat{y_i}}^2}{2{\sigma_i}^2} \tag{2.6.12}$$

3. RESULTS

3.1 Parameter Estimation

The rate constant for phosphorylation and dephosphorylation is acquired by fitting an exponential function to an experimental dataset published by Bouaboula et al[35]. The phosphorylation data is an immunoblotting of CB2 with an antibody showing the percentage change of unphosphorylated receptors in response to a CB2 agonist CP-55940 in CB2 transfected Chinese Hamster Ovary (CHO) cells. Similarly for the dephosphorylation data, only that the agonist is replaced and inverse agonist SR 144528.

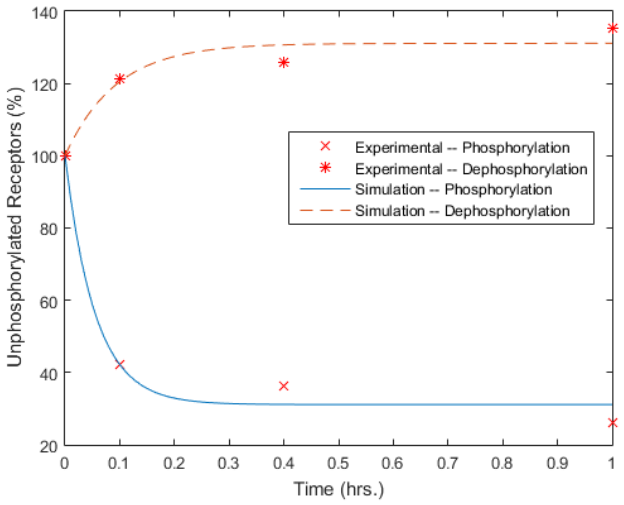

Figure 8. The plot of fitted curve with the experimental datasets.

The loss function plane, shown in Figure 7, demonstrates that there is only one optimal point within the area of interest for the two parameters, and thus we circumvent the potential flaw that Nelder-Mead algorithm might be trapped in a local optimal.

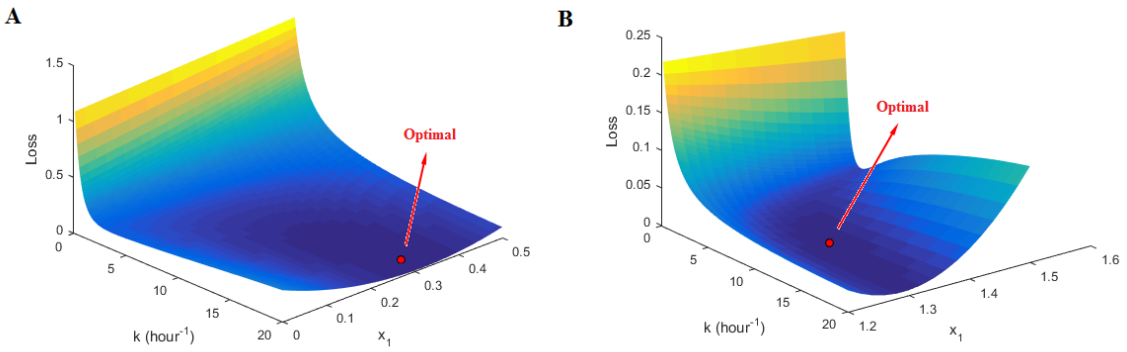

Figure 9. The loss function plane for the exponential functions given the two experimental datasets.

The rate constant for phosphorylation of receptor is estimated to be roughly 20 $hour^{-1} \approx 0.0056$ $second^{-1}$, and that for dephosphorylation is estimated to be roughly 10 $hour^{-1} \approx 0.0028$ $second^{-1}$.

The following is a table for estimated range or value of parameters:

Symbol	Description	Range or Value	Reference
R_t	The total number of receptors. (number of molecules)	2500-50000	[66,70]
k_1	The forward rate constant for receptor activation. (sec^{-1})	1	[66,70]
k_3	The forward rate constant for ligand binding. (M^{-1} sec^{-1})	10^7	[66]
K_{act}	The equilibrium constant for receptor activation. (dimensionless)	0.001-0.1	[3,66]
K_a	The association constant for ligand binding. (M^{-1})	10^8 for agonist; 10^7 for inverse agonist	[39,76]
α	The factor for intrinsic activity of ligand. (dimensionless)	1-100 for agonist; 0.01-0.1 for inverse agonist	[66,70]
k_p	Phosphorylation rate constant. (sec^{-1})	0.00056-0.056	-
k_{dp}	Dephosphorylation rate constant. (sec^{-1})	0.00028-0.028	-
k_{int}	Receptor internalization rate constant. (sec^{-1})	0.001-0.1	[71,72]
k_{rec}	Rate constant for receptor recycling back to cell surface. (sec^{-1})	0.0001-0.01	[71,72]
k_{tr}	Rate constant for receptor transferring from early endosome to recycling endosome. (sec^{-1})	0.00001-0.01	[71]
s	Synthesis and degradation rate. (number of molecules / sec)	0.01-0.1	-

Table 1. The 12 parameters of the model.

3.2 Analytical Solution for Constitutive Steady State

The constitutive steady state is analytically solved using the method mentioned in Section 2.3. The solutions share a common denominator, denoted here as *D*:

$$\begin{aligned} D = {} & k_{dp}k_{int}k_p k_{rec}k_{tr}K_{act} \\ & + k_1\Big(k_{int}k_p k_{rec}k_{tr}K_{act} \\ & + k_{dp}\Big(k_p k_{rec}k_{tr}K_{act} \\ & + k_{int}\Big(k_p k_{tr}K_{act} + k_{rec}\Big(k_p K_{act} + k_{tr}(1+K_{act})\Big)\Big)\Big)\Big) \end{aligned} \tag{3.2.1}$$

Define another factor *F* that will be used in the solutions as:

$$\begin{aligned} F = {} & \Big(s\,k_{dp}k_{int}k_p K_{act} \\ & + k_1\Big(s\,k_{int}k_p K_{act} \\ & + k_{dp}\Big(s\,k_p K_{act} + k_{int}\Big(-R_t k_p K_{act} + s(1+K_{act})\Big)\Big)\Big)\Big) \end{aligned} \tag{3.2.2}$$

In a realistic case, the value for *F* should be negative. The whole solutions for the constitutive steady state are:

$$R_{ss} = k_{dp}k_{int}\big(s\,k_{tr} + k_{rec}(s + R_t k_{tr})\big)\big(k_1 + k_p K_{act}\big)/D \tag{3.2.3}$$

$$R^*_{ss} = k_1 k_{dp}k_{int}\big(s\,k_{tr} + k_{rec}(s + R_t k_{tr})\big)K_{act}/D \tag{3.2.4}$$

$$R_{p,ss} = k_1 k_{dp}k_p\big(s\,k_{tr} + k_{rec}(s + R_t k_{tr})\big)K_{act}/D \tag{3.2.5}$$

$$eeR_{p,ss} = k_1 k_{int}k_p\big(s\,k_{tr} + k_{rec}(s + R_t k_{tr})\big)K_{act}/D \tag{3.2.6}$$

$$eeR_{ss} = -(k_{rec}F)/D \tag{3.2.7}$$

$$reR_{ss} = -(k_{tr}F)/D \tag{3.2.8}$$

It can be easily shown that, at steady state:

$$\frac{R^*_{ss}}{R_{ss}} = \frac{k_1 K_{act}}{k_1 + k_p K_{act}} \tag{3.2.9}$$

$$\frac{R_{p,ss}}{R^*_{ss}} = k_p/k_{int} \tag{3.2.10}$$

$$\frac{eeR_{p,ss}}{R_{p,ss}} = k_{int}/k_{dp} \tag{3.2.11}$$

$$\frac{reR_{ss}}{eeR_{ss}} = k_{tr}/k_{rec} \tag{3.2.12}$$

These ratios can be also acquired by setting $\dot{\vec{r}} = \vec{0}$, implying that the analytical solution is valid as steady state by definition means that the concentration of all involved species remain constant. The simulation using this analytical solution as the initial condition proves the validity of the solution, as shown in Figure 10:

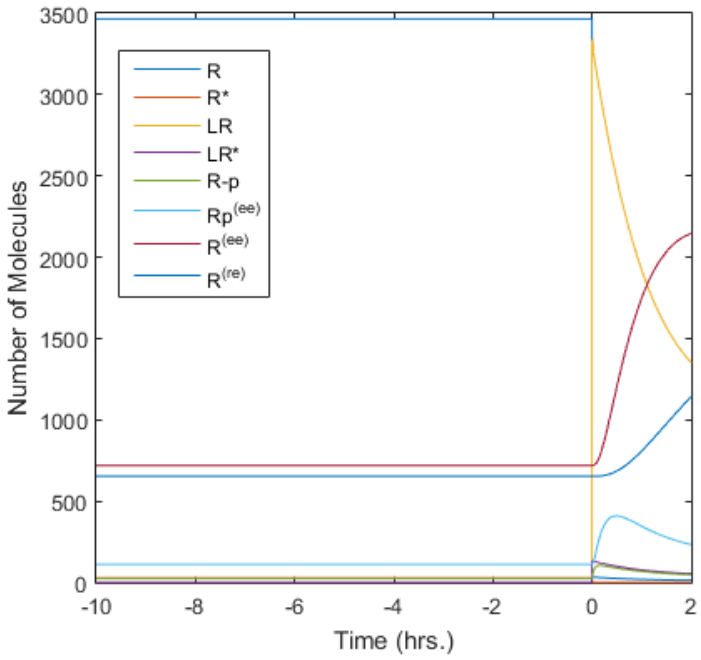

Figure 10. The time course of the simulation result using the analytical solution as initial condition.

Before 0 hour, no ligand is added to the system. At 0 hour, A hypothetical Ligand is added.

3.3 Fitting of The Constitutive Data

20 Markov chains are initialized by running each for 5000 iterations (the first 20% iterations for each chain are burnt-in) to fit the constitutive data as described in Section 2.1 and Section 2.6.2. The plot for best fitting (with the largest likelihood) is shown in Figure 11:

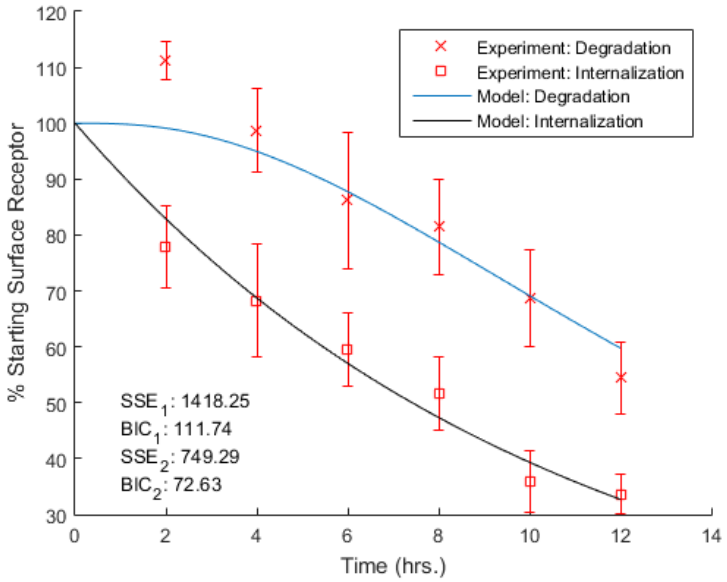

Figure 11. The plot for the best fitting of constitutive data.

SSE_1 and BIC_1 are for the degradation data, SSE_2 and BIC_2 are for the internalization data.

The fit in general is fairly good as indicated by the BIC values, suggesting that under the constitutive condition, the model captures the dynamics of the system. It is worth noting that the relatively high SSE for the degradation data is mainly due to a large discrepancy between the constitutive degradation curve and the model at the 2h time point, which is most likely due to the error in the experimental data, since it exceeds 100% at 2h implying an unreasonable increase in primary antibody-labeled receptors. The delayed degradation indicates that it requires 2-4 hours for surface receptors to get internalized and enter into the degradation compartment under the constitutive condition.

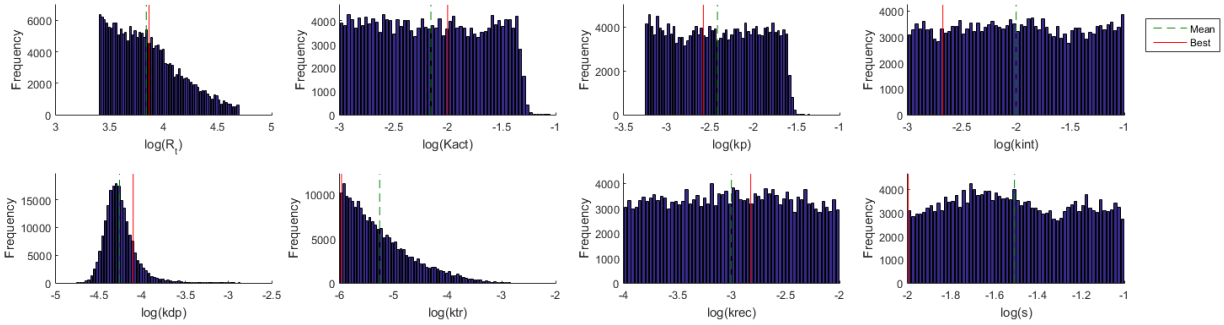

Figure 12. The distribution of MCMC-sampled points on the 8 independent parameters.

The posterior probability distribution $P(\boldsymbol{\theta}|\boldsymbol{D})$ revealed by the MCMC sampling technique, as shown in Figure 12, shows that these two data offer little constraints on most parameters, as the

obvious flat distribution, except for k_{dp}, the rate constant for dephosphorylation of internalized receptors, as well as k_{tr}, the rate constant for transferring receptors from early endosome to the recycling endosome. This suggests that constitutively the receptor dephosphorylation and trafficking is rather slow.

3.4 Simultaneous Fitting of Constitutive and Ligand Treatment Data

The model is fitted to constitutive and ligand treatment data simultaneously, to ensure that the model with the resulted parameters satisfies both observed constitutive and ligand-induced behaviors. The fitting is generally good for ligand treatment data, but poor for the constitutive data (large SSEs for both degradation and constitutive internalization data), as shown in Figure 13.

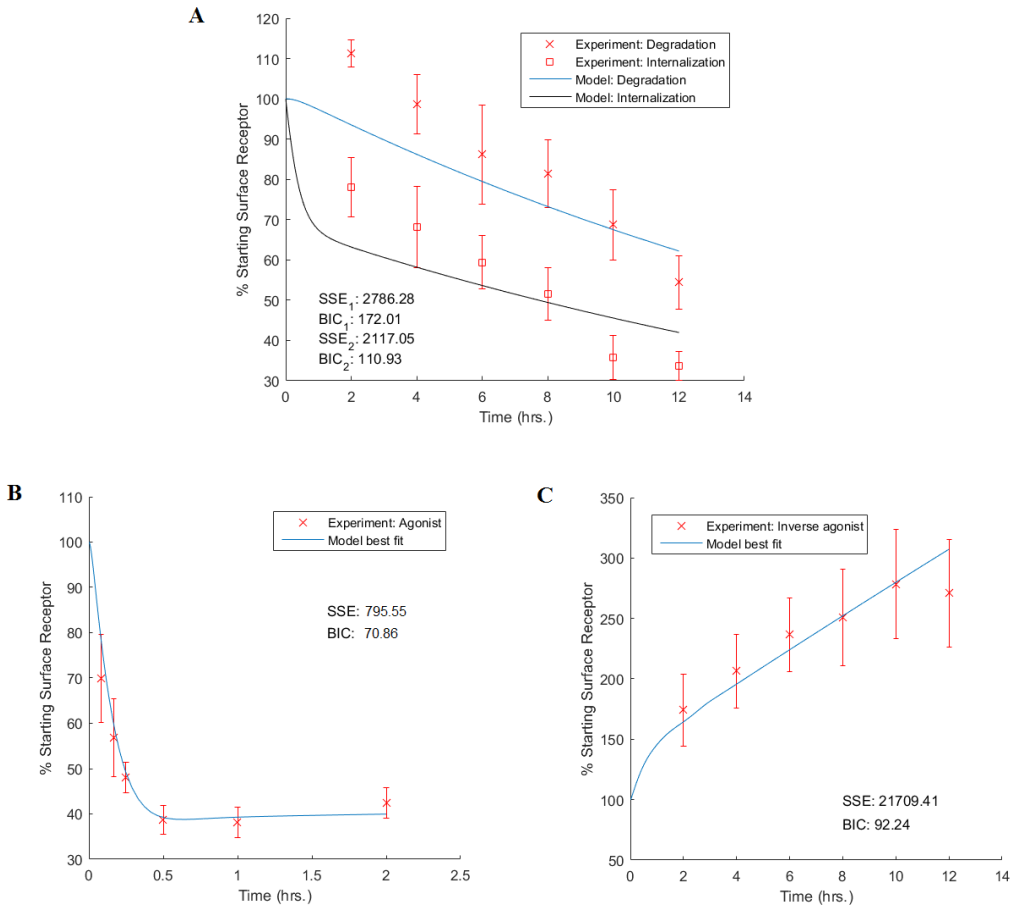

Figure 13. The plot for the best fitting of four datasets.

In (A), SSE_1 and BIC_1 are for the degradation data, SSE_2 and BIC_2 are for the internalization data.

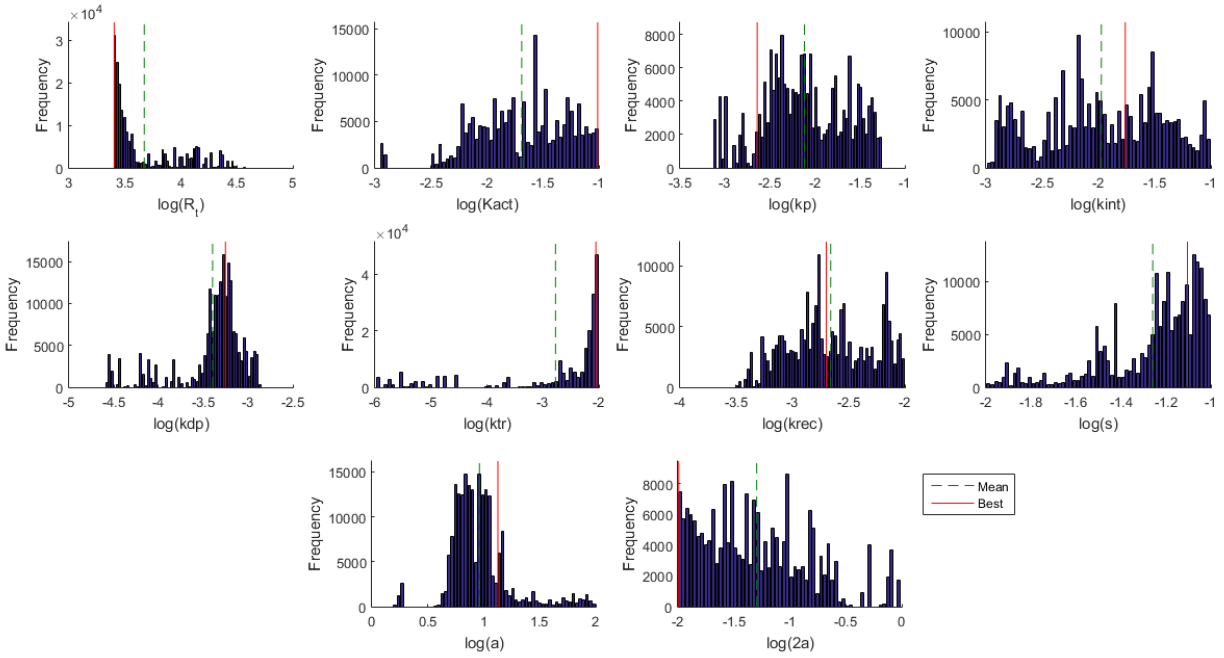

Figure 14. The distribution of MCMC-sampled points on the 10 independent parameters.

To test if this is due to a predominately high likelihood bias towards the fitting for ligand treatment data, a second fitting with 5× weight on the likelihood for constitutive data is run, and the results are shown in Figure 15.

As shown in the Figure 15, the weighted fitting procedure, even though performed well on constitutive data, fits ligand treatment data poorly, indicated by an SSE of 6055.53 for agonist data and that of 90963.92 for inverse agonist data, respectively, suggesting that the model indeed cannot satisfy both data simultaneously. Combining with the results shown in Figure 13, these data strongly suggests that the current model cannot capture the dynamics of the true system under different conditions, and that the ligand-induced receptor endocytosis and trafficking is very likely to be intrinsically different processes than that under constitutive condition.

By comparing the distributions shown in Figure 12 and Figure 14, it is easy to see that first, the distribution for many parameters are more restricted, thanks to information provided by the ligand treatment data; and second, among all the processes, the transfer of receptors from early endosome to recycling endosome, as well as the dephosphorylation of internalized receptors are the two processes with the most noticeable difference. This supports the idea that, as reported in various literatures, ligands can penetrate the cell membrane, or be internalized along with the receptors to affect receptor trafficking inside the cell. The model needs to be revised to account for and test this finding.

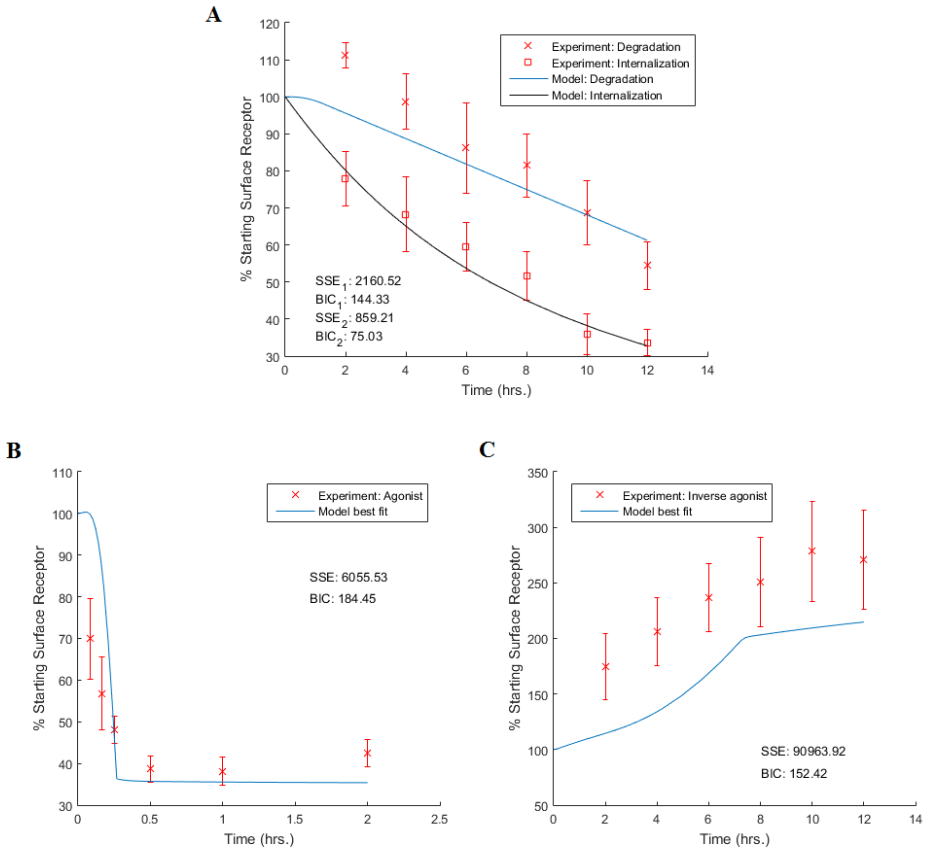

Figure 15. The plot for the best 5× constitutive data-weighted fitting.

In (A), SSE_1 and BIC_1 are for the degradation data, SSE_2 and BIC_2 are for the internalization data.

3.5 Simultaneous Fitting Using Revised Model

To account for the new assumption that ligand-treatment can affect and alter the rate of processes that occur after receptor activation, an additional parameter ε is added as a multiplier of k_{tr} due to ligand's effects. The range of ε is estimated to be 10-1000 according to the distribution plot for k_{tr} shown in Figure 12 and Figure 14. As previous, 50 Markov chains with different initial positions are each run for 5000 iterations. The results for best fitting curve as well as the distributions are shown as follows in Figure 16 and Figure 17:

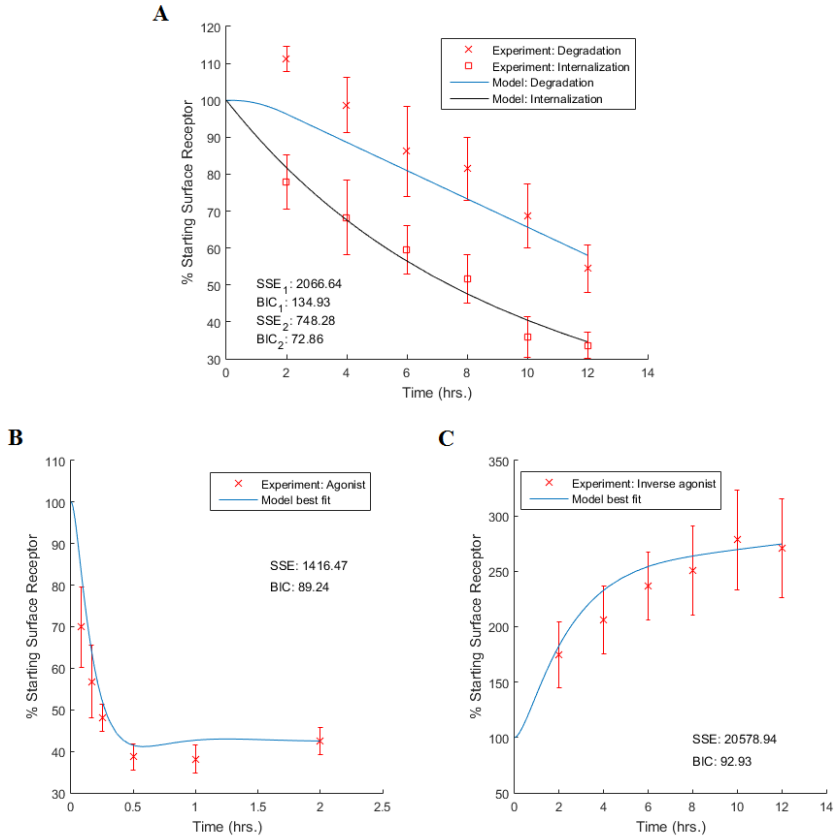

Figure 16. The plot for the best 2× constitutive data-weighted fitting using the revised model.

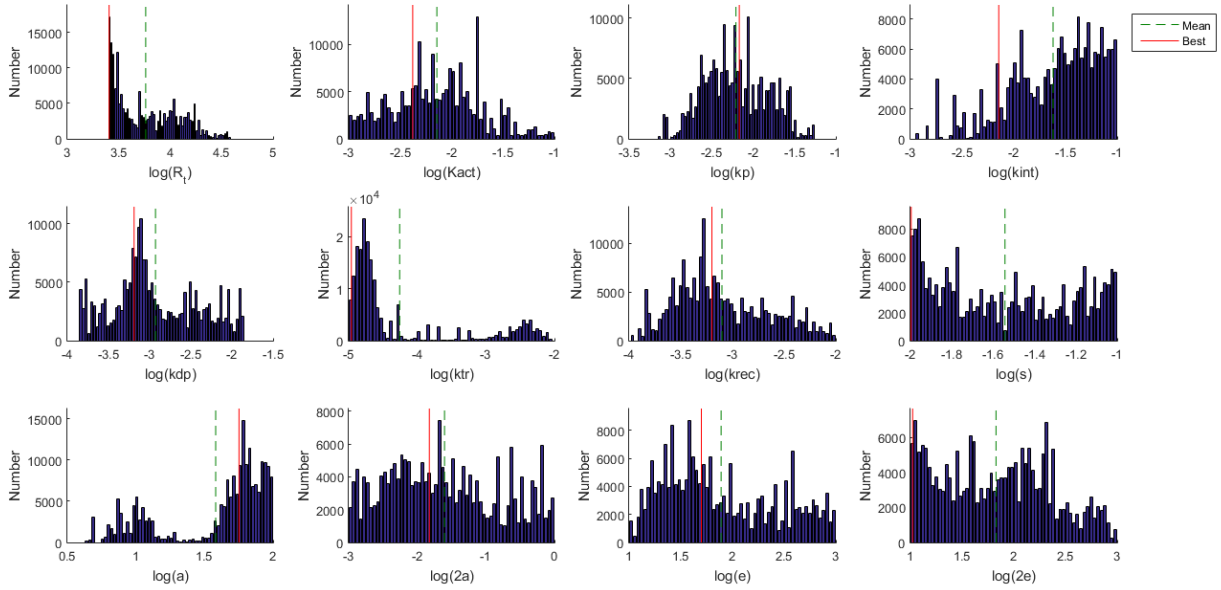

Figure 17. The distribution of MCMC-sampled points on the 12 independent parameters.

The fitting results in general are much better than those in Section 3.4. Particularly for the fitting of constitutive data, the SSE (2066.64 for degradation data, and 748.28 for constitutive internalization data) is slightly better than the SSE (2160.62 for degradation data, and 859.21 for constitutive internalization data) from the previous fitting where 5× weights are added to the likelihood for fitting of constitutive data, but not as good as the SSE (1418.25 for degradation data, and 749.29 for constitutive internalization data) from the first fitting which is under only constitutive condition. BIC tends to penalize the addition of new parameters, but still we see a general decrease in almost all BICs in the fitting using revised model, with the exception that the BICs of fitting for ligand treatment data are larger when compared to that shown in Figure 13.

The distribution of MCMC samples on independent parameters show that for parameters R_t, k_p, k_{dp}, k_{tr}, k_{rec}, and α, there are rather restricted constraints provided by the data, and for the rest of the parameters, there are also certain degrees of non-uniformity in their distribution. This suggests that the four experimental datasets are fairly informative and that many parameters can be sufficiently estimated through this data fitting procedure.

3.6 Summary of Data Fitting Results

Here I summarize all the fitting results in this table:

	Fit 1	**Fit 2**	**Fit 3**	**Fit 4**
SSE_1	1418.25	2786.28	2160.52	2066.64
BIC_1	111.74	172.01	144.33	134.93
SSE_2	749.29	2117.05	859.21	748.28
BIC_2	72.63	110.93	75.03	72.86
SSE_a	-	795.55	6055.53	1416.47
BIC_a	-	70.86	184.45	89.24
SSE_i	-	21709.41	90963.92	20578.94

BIC_i	-	92.24	152.42	92.93

Table 2. Summary of all data fitting results.

Fit 1: Original model, only constitutive data, no weight;

Fit 2: Original model, constitutive data + ligand treatment data, no weight;

Fit 3: Original model, constitutive data + ligand treatment data, 5× weight on constitutive data;

Fit 4: Revised model, constitutive data + ligand treatment data, 2× weight on constitutive data;

SSE_a, BIC_a: For agonist treatment data;

SSE_i, BIC_i: For inverse agonist treatment data.

Poor fits are marked in red.

4. DISCUSSION

4.1 Significance of the Study

GPCRs are one of the most popular target for drug intervention, but its desensitization phenomenon has been a problem for many treatment strategies. For asthma treatment, the desensitization of β_2 adrenergic receptor is suspected to be the main reason for its ineffectiveness. In the field of neuropharmacology, desensitization of opioid receptors is considered to be a major player in development of opioid tolerance. CB2 receptors as new targets for treating neural inflammation, Alzheimer's disease, and other pathological conditions, understanding its endocytosis and intracellular trafficking is then essential for design of effective drug treatment strategies.

GPCR desensitization is composed of a series of temporally sequential events, involving phosphorylation of receptors on the membrane, binding of arrestin, and internalization. The kinetics of the whole system enables GPCR to respond to ligand differently on two time scales. The acute effect of an arbitrary agonist leads to the activation of the whole system, while chronically the response vanishes and sometimes reverses. This time-dependent phenomenon makes it interesting and important to develop a kinetic model that can be used to study its temporal behavior and make predictions. However, such models are rather few for GPCR and not as complete as those for other biological systems, e.g. epidermal growth factor receptors (EGFR)[86] or high-affinity IgE receptor (FcεRI)[87].

Given six published experimental datasets, this thesis aims to develop a simplistic model for CB2 endocytosis and intracellular trafficking, and hopefully provide new insights for understanding and modeling this particular system as well as other GPCRs.

4.2 Mechanism Based Modeling of CB2 Endocytosis and Trafficking

New findings unraveled by experiments on GPCR signaling and regulation change our understanding of the system all the time. The concept of "intrinsic efficacy" for GPCR has always been changing subtly but decisively. The two-state model for GPCR is intuitively easy to accept, and capable of explaining most experimental observations, where receptors are spontaneously activated, and the intrinsic efficacy of a ligand is exhibited via its ability and preference to bind to the active or inactive state. This point of view, even though true to some extent, is challenged by

the observation that there is more than one active state for most GPCRs. For instance, it has been shown that the reduced response caused by a partial agonist for β_1-adrenergic receptor is due to a less potent active state it induced, which is distinct from the active state induced by a full agonist[88]. The finding of "protean agonists" implied that the ligand-stabilized active state can be an "active state" that is less potent than the constitutive active in terms of G-protein coupling, and, the subtle differences among the various conformational states of the GPCR make the response of a ligand sensitive to conditions including receptor and G-protein expression level, as well as constitutive activity[66,89].

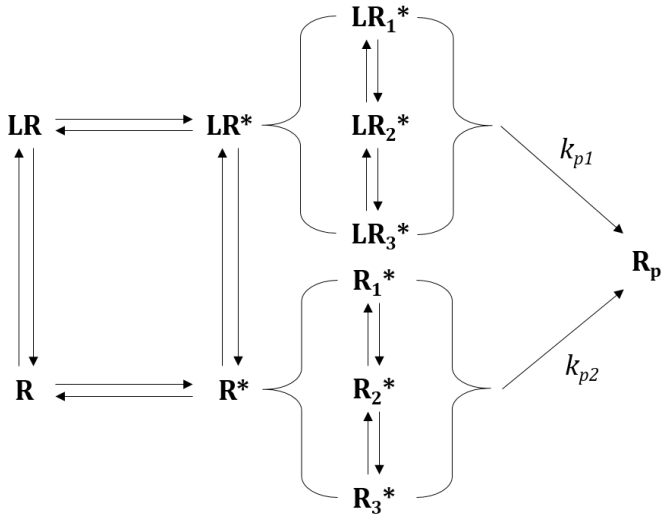

Figure 18. A diagram showing how the ODE model can incorporate multiple active states of receptors.

Seemingly, this ODE model does not include multiple active states and seems not to be able to account for the above concepts, as there are only R* and LR*, the spontaneous active state and ligand-stabilized active state. However, considering that, if R* represents a subset of multiple active states, among which the transition is fast enough that can be seen as a whole, the minor differences in the conformations of various spontaneous active state might not be that important for kinetic models. Similarly, a single symbol LR* can amount to a subset of ligand-bound active states, and by adding a multiplier for the phosphorylation rate, as we did for k_{tr} in Section 3.5, the ligand-bound active state can be phosphorylated via a slower or faster process.

The ODE model does not explicitly model the different trafficking route for ligand-bound receptors and free receptors because this will lead to additional modeling efforts for ligand association and dissociation inside the cell that requires the knowledge of endosome volume. Instead, to account for ligands' effects inside the cell, the rate constant for affected processes are

multiplied with a factor which will be one in the absence of ligand molecules. Arrestin binding and the endocytosis process are modeled as a single process in this model, since there is no data allowing for such differentiation. Such simplification strategy is also used by many other mathematical models.

4.3 Effects of Ligands on CB2 Trafficking

The phenomenon that many GPCR are constitutive active not only permits the action of inverse agonists, but also is suspected to be one of the reasons that some GPCR undergo constitutive phosphorylation and internalization. For CB2, this hypothesis is supported by the data that the using of inverse agonist leads to increase in the number of unphosphorylated as well as surface receptors[35,39]. The first ODE model is built based on the assumption that the ligands' effects on CB2 endocytosis and trafficking can be purely attributed to their ability to shift the activation equilibrium of the receptor, which have no effect on other events posterior to receptor activation. Fitting of the model to the experimental data, as shown in Section 3.4, however, suggests that this hypothesized mechanism cannot fully explain all the data.

The model is then revised by incorporating the possibility that ligands can affect receptor endocytosis and trafficking after receptor activation and inside the cell by either directly changing the conformation of the bound receptor into a better substrate for phosphatase, or somehow activating the phosphatase. This idea is also proposed in Bouaboula et al.'s experimental study, but yet to be verified[35]. According to the parameter distribution plot from data fitting, two processes are found to be the most affected by ligand treatment, which are the transfer of receptors from early endosome to recycling endosome, and the dephosphorylation of internalized receptors. A second fitting using a revised model where the rate for the transfer process is multiplied by a factor under ligand treatment condition shows an improved performance of the model on the datasets. It is worth pointing out that it is also easy to add another factor to alter the dephosphorylation along with the transfer process and could enhance the fitting performance further, but rather pointless as we could do this to all the reactions to make the model behaves totally independently under ligand treatment or constitutive condition, and yet the conclusion will not change.

An interesting relevant phenomenon that ligand stimulation affects receptor trafficking property is found in the vascular endothelial growth factor 2 (VEGFR2) signaling pathway.

Constitutively internalized VEGFR2 recycles through Rab4-mediated fast recycling pathway[90,91], whereas the VEGF-VEGFR2 complex undergoes a Rab11-mediated recycling pathway, promoted by a co-receptor neuropilin-1 (NRP1)[90,92]. Given the knowledge that CB2 trafficking is not affected by variation of Rab4[39], I postulate that constitutively CB2 experiences slow or effectively no recycling, while the activation of CB2 by ligand, either an agonist or inverse agonist, activates or targets the receptor to the Rab-11 recycling pathway. This is also backed by the data that the introduction of constitutively active or dominant negative Rab11 alters the AM630 induced recycling, but not the constitutive trafficking of CB2[39].

4.4 Limitations

Despite that the revised model captures the dynamics of the system quite well, there are still uncertainties and questions remained to be determined or answered. The data-constrained model demonstrates that a simple assumption that ligands regulate receptor endocytosis and recycling does not suffice to explain the four experimental datasets published by Grimsey et al. simultaneously[39], and that the transfer of receptor from early endosome to recycling endosome, as well as the dephosphorylation of internalized receptors are the two processes suspected to be modulated by ligand, but such model cannot reflect the detailed molecular mechanism through which the ligand exhibits such effects. In addition, a study of CB receptors using primary human cells has shown that, unlike what happened in the transfected cells, they do not undergo internalization upon agonist treatment, but are transported between cytoplasm and cell membranes via ligand-independent mechanisms[93]. This would impair the relevance of not only this work, but also all the previous experimental works that are done in transfected animal cells.

As mentioned in Section 4.2, GPCRs are complicated systems that many details regarding their signaling, endocytosis, and trafficking are still unknown. Our model, even though designed specifically for the data to be explained and based upon references from other relevant modeling studies, is too simplistic to have great prediction power. Certainly, a much more detailed model would require a much more detailed dataset to be used as validations, which is rather scarce for GPCRs, especially the CB2 receptor.

For the goal of this project, an alternative to data fitting is parameter synthesis techniques, which are techniques that can identify an area of parameters with which the model will show a certain desirable or undesirable behavior[94]. Sampling strategy, such as MCMC, even though is

much easier to implement, suffers problems including inefficient and insufficient sampling, and uncertainty of convergence. Parameter synthesis specifies “behavior” or “event” of a model using logics, instead of continuous data points. The algorithm first approximates the reachable set, a cluster of behaviors that can be possibly reached by the model with parameters arbitrarily chosen from the parameter space, by using a finite number of simulated trajectories and sensitivity analysis, and then classifies each parameter subset as either satisfying the specification or not by computing the intersection between the reachable set and the specified region. Therefore, if a desirable behavior is not present, then the intersection will be an empty set, meaning the model cannot explain the experimental observation.

4.5 Future Prospective

A more comprehensive dataset quantifying time courses for receptors in all compartments, early endosome, late endosome, recycling endosome, as well as the cell membrane will provide much more information for building a complete model. 3D imaging of receptor distribution in cellular substructures could facilitate the development of a spatial model. Therefore, the prerequisite for the most promising improvement for my work will be more informative and quantitative biological data. This can be possibly done by either designing the experiment in our laboratory or through collaborations.

It is crucial to know how the output, surface receptor expression level, is sensitive to the variation of each parameter. Many biological systems are known to be robust to changes in cellular conditions due to environmental noise, so it is not necessarily true that parameters with the largest variation would be the most important determinant for the model. Meanwhile, in the process of model development, the value and range for many parameters are determined through some data-guided heuristic approach, and this can be done in a much more systematic manner by understanding the whole picture of how each parameter contributes to the final behavior of the model. A global sensitivity analysis, e.g. partial rank correlation coefficients (PRCC) or elementary effects (EE), can be used to resolve such issue.

For this particular study, I do not see any necessity to use stochastic simulation method, as all the species are abundant in each compartment, and there is no evidence showing obvious traits for stochastic effects in this system. Future models, however, especially if receptor expression and

CME are modeled mechanistically, might need to consider stochastic behaviors, in which case stochastic simulation algorithms, e.g. Gillespie algorithm, will be needed.

The final goal for such model, after extensive validation and modification, is to not only explain how the whole system works, but also predict how the response of the system will change as a result of certain variations of involved biological processes. These variations can be due to genetic variations, disease status, or environmental stimuli, including medications and antigens.

APPENDIX A. IMPLEMENTATION DETAILS FOR MCMC

In Section 2.6.2, several probability functions are briefly mentioned, without detailed explanation of their practical meaning. In this appendix, we will discuss the MCMC theory with further details and attempt to connect abstract mathematical formulas to the real problem we have.

Metaphorically we can imagine a biological system as a machine that produces data. Since machines are never perfect, so the data they produced contain *noise*. Of course in the sense of experimental data, noise sometimes comes from the mean of measurement, not necessarily from the biological system itself, but for now, let us keep that simple mindset for convenience. Mathematical models are descriptions of such system, and in the case of deterministic models, they try to mimic the real biological system and are noise-free. How accurate, or how close a kinetic model is to the real system depends on the architecture, (i.e. how species are wired up) and the value of each parameter. Therefore the task for parameter estimation algorithms, including MCMC techniques, is to search for a parameter set that maximizes the accuracy of the model, assuming the architecture is "correct" or close enough.

In reality, however, we will not be able to know how a biological system really works. Typically, all we have are some experimental data $\boldsymbol{D}$ that generated by the system – evidences, and some facts or speculations on how the system works, which sometimes lead to a deterministic kinetic model M – the hypothesis. With different values for the parameters $\boldsymbol{\theta}$, the model M behaves differently, meaning that the model M is a function of $\boldsymbol{\theta}$. Even if we can find a parameter set $\boldsymbol{\theta_i}$ making the hypothesis $M(\boldsymbol{\theta_i})$ fits the evidences $\boldsymbol{D}$ extremely well, we can only say it is very likely that the real system works the same as $M(\boldsymbol{\theta_i})$**.** Statistically we say, given the evidences $\boldsymbol{D}$, the probability that the hypothesis $M(\boldsymbol{\theta_i})$ is true is high, but there is still some probability that with another parameter set, say, $\boldsymbol{\theta_j}$, the hypothesis $M(\boldsymbol{\theta_j})$ is true. This probability we are describing now is the very posterior probability $P(\boldsymbol{\theta}|\boldsymbol{D})$. With this mindset, I summarized the practical meaning for all probability functions in the following table:

Symbol	Terminology	Practical Meaning
$P(\boldsymbol{\theta}\|\boldsymbol{D})$	Posterior Probability	The probability that $M(\boldsymbol{\theta})$ is true, given data $\boldsymbol{D}$.
$P(\boldsymbol{D}\|\boldsymbol{\theta})$	Likelihood	The probability that $\boldsymbol{D}$ are generated, if $M(\boldsymbol{\theta})$ is true.
$P(\boldsymbol{\theta})$	Prior Probability	The probability that $M(\boldsymbol{\theta})$ is true, without knowing $\boldsymbol{D}$.
$P(\boldsymbol{D})$	Marginal Likelihood	The probability that $\boldsymbol{D}$ are generated, without knowing $M(\boldsymbol{\theta})$.

Table 3. Summary of Probability Functions.

The ultimately goal for MCMC is to sample random points from distribution of posterior probability $P(\boldsymbol{\theta}|\boldsymbol{D})$. But as discussed in Section 2.6.2, computing $P(\boldsymbol{\theta}|\boldsymbol{D})$ is intractable for most complex systems, and that is why we need to use Eq.2.6.3 instead to approximate $P(\boldsymbol{\theta}|\boldsymbol{D})$ by generating samples from the product of likelihood and prior probability distribution. The likelihood for a single data point y_i can be well defined, assuming Gaussian noises:

$$P(y_i|\boldsymbol{\theta}) = \frac{1}{\sqrt{2\pi}\sigma_i}\exp\left[-\frac{\left(y_i - x(t_i;\boldsymbol{\theta})\right)^2}{2{\sigma_i}^2}\right] \tag{A.1}$$

This formula describes the probability that y_i is sampled from a Gaussian distribution with a mean of $x(t_i;\boldsymbol{\theta})$, the simulation result generated by $M(\boldsymbol{\theta})$ at i-th time point t_i, and a variance of σ_i. The likelihood for all data points $\boldsymbol{D} = \{y_i|i = 1, 2, \dots, n\}$ can be calculated as the product of Eq.A.1 for all elements in $\boldsymbol{D}$, supposing that the sampling events are independent, which leads to Eq.2.6.5. In practical, the calculation of likelihood is done by using the following formula, which can be readily shown to be equivalent to Eq.2.6.5:

$$P(\boldsymbol{D}|\boldsymbol{\theta}) = \left(\prod_i \frac{1}{\sqrt{2\pi}\sigma_i}\right)\left(\exp\left[-\frac{1}{2}\sum_i\left(\frac{y_i - x(t_i;\boldsymbol{\theta})}{\sigma_i}\right)^2\right]\right) \tag{A.2}$$

The product in the first pair of brackets can be omitted, since we are interested in the ratio of likelihood functions $P(\boldsymbol{D}|\boldsymbol{\theta}')/P(\boldsymbol{D}|\boldsymbol{\theta})$, as shown by Eq.2.6.7, while this product is a constant for all $\boldsymbol{\theta}$. For the exponential function in the second pair of brackets, the exponent is first calculated, and when calculating the ratio of likelihood functions, the difference between the exponents of the

two likelihood function is calculated, to avoid numerical problems when the two likelihoods are too small that they exceed the lower bound of the range for the computer to store a float. Specifically, if we denote the summation part of the exponent in Eq.A.2 as $Z(\boldsymbol{\theta})$, from Eq.2.6.7, we can compute the ratio as:

$$\frac{P(\boldsymbol{D}|\boldsymbol{\theta}')}{P(\boldsymbol{D}|\boldsymbol{\theta})} = \exp\left[-\frac{1}{2}\left(\sum_i \left(\frac{y_i - x(t_i;\boldsymbol{\theta}')}{\sigma_i}\right)^2 - \sum_i \left(\frac{y_i - x(t_i;\boldsymbol{\theta})}{\sigma_i}\right)^2\right)\right]$$

$$= \exp\left[-\frac{1}{2}\big(Z(\boldsymbol{\theta}') - Z(\boldsymbol{\theta})\big)\right] \tag{A.2}$$

For this study, we have a total of for datasets, and if we call degradation data as data 1, constitutive internalization data as data 2, agonist treatment data as data *a*, and inverse agonist treatment data as data *i*, then we have:

$$Z(\boldsymbol{\theta}) = Z_1(\boldsymbol{\theta}) + Z_2(\boldsymbol{\theta}) + Z_a(\boldsymbol{\theta}) + Z_i(\boldsymbol{\theta}) \tag{A.3}$$

Sometimes due to practical issues, we have certain terms in Eq.A.3 that are extremely large making them dominate the value of $Z(\boldsymbol{\theta})$. For example in Section 3.4 we found that $Z_1(\boldsymbol{\theta}) + Z_2(\boldsymbol{\theta}) \ll Z_a(\boldsymbol{\theta}) + Z_i(\boldsymbol{\theta})$, therefore $Z(\boldsymbol{\theta}) \approx Z_a(\boldsymbol{\theta}) + Z_i(\boldsymbol{\theta})$. To overcome this problem, I assign a weight *w* to the small terms to make it larger artificially:

$$Z(\boldsymbol{\theta}) = w\big(Z_1(\boldsymbol{\theta}) + Z_2(\boldsymbol{\theta})\big) + Z_a(\boldsymbol{\theta}) + Z_i(\boldsymbol{\theta}) \tag{A.4}$$

We used $w = 5$ in the third fit, and $w = 2$ in the fourth fit.

APPENDIX B. CORE CODES

The indices for each species and parameter are defined in a script **Initialize.m**:

```
%% Species
inited = 1;
global R Rs LR LRs Rp eeRp eeR reR...
    names keys n_species
%% Species
R = 1;
Rs = 2;
LR = 3;
LRs = 4;
Rp = 5;
eeRp = 6;
eeR = 7;
reR = 8;

names = {'R' 'R*' 'LR' 'LR*' 'R-p' 'Rp^{(ee)}' 'R^{(ee)}', 'R^{(re)}'};
keys = {'R' 'Rs' 'LR' 'LRs' 'Rp' 'eeRp' 'eeR' 'reR'};

n_species = 8;

%% Parameter list
global ik1 iKact ik3 iKa ia ...
ikp ikint ikdp iktr ikrec ikre5 is iRt iL...
ie ...
n_params knames

% Rate & Equilibrium constants
ik1 = 1; iKact = 2; ik3 = 3; iKa = 4; ia = 5;
% GRK & recycling module
ikp     =   6;
ikint   =   7;
ikdp    =   8;
iktr    =   9;
ikrec   =   10;
ikre5   =   11;
is      =   12;
% concentrations
iRt     =   13;
iL      =   14;
ib      =   15;
ic      =   16;
id      =   17;
ie      =   18;
ig      =   19;
ih      =   20;

n_params    =   20;
knames = {'k1' 'Kact' 'k3' 'Ka' 'a'...
```

```
    'kp' 'kint' 'kdp' 'ktr' 'krec' 'kre4' 's' 'R_t' 'iL' 'b', 'c', 'd', 'e',
'g', 'h'};

%% Ligand2 Parameters
global i2a i2Ka i2e n_params2 knames2
i2a    =  n_params + 1;  % Agnoist
i2Ka   =  n_params + 2;
i2e    =  n_params + 3;
n_params2 = n_params + 3;
knames2 = cat(2, knames, {'2a' '2Ka', '2e'});

%% Constants
global M nM uM V VM NA Mm nMm uMm VE Me nMe uMe
% Avogadro's number
NA      =  6.02e23;           % mol
nano    =  1e9;
mu      =  1e6;
mag     =  1e3;
% Volumes
V       =  1.77e-12;          % Cell Volume, 1fL -> 1e-15L
VM      =  V/100;             % Membrane Volume
VE      =  V/1000;            % Endosome Volume
% Unit conversions
M       =  V*NA;
nM      =  M/nano;
uM      =  M/mu;
% Unit conversions
Mm      =  VM*NA;
nMm     =  Mm/nano;
uMm     =  Mm/mu;
% Unit conversions
Me      =  VE*NA;
nMe     =  Me/nano;
uMe     =  Me/mu;
```

The ODEs are written as MATLAB codes and solved in function `solveodes`:

```
function [T,Y,terminated] = solveodes(C, tspan, Parameters, solver)
% Solve ODEs numerically
%######################## Species mapping list ############################
global R Rs LR LRs Rp eeRp eeR reR
global ik1 iKact ik3 iKa ia ...
       ikp ikint ikdp iktr ikrec ikre5 is iL ie
%########################## Parameters list ##############################
k1      = Parameters(ik1);
Kact    = Parameters(iKact);
k3      = Parameters(ik3);
Ka      = Parameters(iKa);
a       = Parameters(ia);
kp      = Parameters(ikp);
kint    = Parameters(ikint);
kdp     = Parameters(ikdp);
```

```
ktr     = Parameters(iktr);
krec    = Parameters(ikrec);
kre5    = Parameters(ikre5);
s       = Parameters(is);
L       = Parameters(iL);
e       = Parameters(ie);
%######################## Differential Equations ########################
%options = odeset('NonNegative', 1:numel(C));
%[T, Y] = solver(@diffeqts, tspan, C, options);
[T, Y] = solver(@diffeqts, tspan, C);

if (T(end) < tspan(end) - 0.5)
    fprintf(':\n');
    terminated = 1;
else
    fprintf('.');
    terminated = 0;
end

function [ dc ] = diffeqts( t, c )
% Differential Equations for the model;
% input: t -- time; c -- concentrations for species
% output: dc -- dc/dt
if c(eeR) >= 100
    deg = s;
else
    deg = s/100 * c(eeR);
end

dc = zeros(size(c));

dc(R) = - k1 * c(R) + (k1/Kact) * c(Rs) - k3 * L * c(R) + (k3/Ka) * c(LR)...
    + krec * c(reR) + kre5 * c(eeR) + s;
dc(Rs) = k1 * c(R) - (k1/Kact) * c(Rs) - a*k3 * L * c(Rs) + (k3/Ka) *
c(LRs) ...
    - kp * c(Rs);
dc(LR) = - a*k1 * c(LR) + (k1/Kact) * c(LRs) + k3 * L * c(R) - (k3/Ka) *
c(LR);
dc(LRs) = a*k1 * c(LR) - (k1/Kact) * c(LRs) + a*k3 * L * c(Rs) - (k3/Ka) *
c(LRs) ...
    - kp * c(LRs);
dc(Rp) = kp * c(Rs) + kp * c(LRs) - kint * c(Rp);
dc(eeRp) = kint * c(Rp) - kdp * c(eeRp);
dc(eeR) = kdp * c(eeRp) - e * ktr * c(eeR) - kre5 * c(eeR) - deg;
dc(reR) = e * ktr * c(eeR) - krec * c(reR);
end

end
```

To simulate the dynamics of labeled species, as discussed in Section 2.4, another function `solveodes_nosynth`, is written with no receptor synthesis term but otherwise the same as `solveodes`. For simplicity, the codes for `solveodes_nosynth` are not attached here.

The calculation of constitutive steady state is implemented based on analytical solutions shown in Section 3.2:

```
function [ c0 ] = initConc( Parameters )
%INITCONC calculate constitutive steady state

global R Rs LR LRs Rp eeRp eeR reR n_species
global ik1 iKact ...
       ikp ikint ikdp iktr ikrec ikre5 is iRt
k1      = Parameters(ik1);
Kact    = Parameters(iKact);
kp      = Parameters(ikp);
kint    = Parameters(ikint);
kdp     = Parameters(ikdp);
ktr     = Parameters(iktr);
krec    = Parameters(ikrec);
kre5    = Parameters(ikre5);
s       = Parameters(is);
Rt      = Parameters(iRt);

den = kdp * kint * kp * krec * (kre5 + ktr) * Kact ...
    + k1 * (kint * kp * krec * (kre5 + ktr) * Kact ...
    + kdp * (kp * krec * (kre5 + ktr) * Kact ...
    + kint * (kp * ktr * Kact + kre5 * krec * (1 + Kact) ...
    + krec * (kp * Kact + ktr * (1 + Kact)))));

c0 = ones(n_species, 1) / den;
kcom = Rt * kre5 * krec + s * ktr + krec * (s + Rt * ktr);
c0(R) = c0(R) * kdp * kint * (k1 + kp * Kact) * kcom;
c0(Rs) = c0(Rs) * k1 * kdp * kint * Kact * kcom;
c0(LR) = 0;
c0(LRs) = 0;
c0(Rp) = c0(Rp) * k1 * kdp * kp * Kact * kcom;
c0(eeRp) = c0(eeRp) * k1 * kint * kp * Kact * kcom;
kcom2 = kdp * kint * kp * s * Kact ...
    + k1 * (kint * kp * s * Kact + kdp * (kp * s * Kact ...
    + kint * (-Rt * kp * Kact + s * (1 + Kact))));
c0(eeR) = c0(eeR) * (-krec * kcom2);
c0(reR) = c0(reR) * (-ktr * kcom2);

end
```

The ranges for each parameter and other preparations for running MCMC are defined and coded in **MCMC2.m**:

```
Initialize();
global ik1 iKact ik3 iKa ia ...
ikp ikint ikdp iktr ikrec ikre5 is iRt iL ie...
i2a i2Ka i2e n_params2
```

```
%% Parameter Ranges
rangs = zeros(n_params2, 2);
% Concentrations
rangs(iL,:) = 1e-6 * [1, 1];
rangs(iRt,:) = 5000 * [0.5, 10];
% Rate & Equilibrium constants
rangs(ik1,:) = [1 1];
rangs(ik3,:) = 1e7 * [1 1];
rangs(iKact,:) = [0.001 0.1];
rangs(iKa,:) = 1e8 * [1 1];
rangs(ia,:) = [1 100];
rangs(ie,:) = [1 1000];
rangs(i2Ka,:) = 1e7 * [1 1];
rangs(i2a,:) = [0.01 1];
rangs(i2e,:) = [10 1000];
% GRK & recycling module
rangs(ikp,:)       =   0.0056 * [0.1 10];     % GRK phosphorylates receptor
rangs(ikdp,:)      =   0.0014 * [0.1 10];     % phosphotase dephosphorylates
receptor
rangs(ikint,:)     =   [0.001 0.1];           % internalize
rangs(ikrec,:)     =   [0.0001 0.01];         % recycle via rab11
rangs(iktr,:)      =   [0.00001 0.01];        % rab5 -> rab11
rangs(ikre5,:)     =   0 * [1, 1];            % recycle via rab5
% Synthesis & Degradation
rangs(is,:) = 0.1 * [0.1, 1];

%% Parameter Scale
% 0 for log, 1 for linear
scale = zeros(n_params2, 1);

%% Parameter Selection
sele = zeros(n_params2, 1);
sele(iL)  =   0;
sele(iRt)  =   1;
% Rate & Equilibrium constants
sele(ik1) = 0;
sele(ik3) = 0;
sele(iKact) = 1;
sele(iKa) = 0;
sele(ia) = 1;
sele(ie) = 1;
sele(i2Ka) = 0;
sele(i2a) = 1;
sele(i2e) = 1;
% GRK & recycling module
sele(ikp)       =   1;    % GRK phosphorylates receptor
sele(ikdp)        =   1;    % phosphatase dephosphorylates receptor
sele(ikint)       =   1;    % internalize
sele(ikrec)       =   1;    % recycle
sele(iktr)       =   1;
sele(ikre5)       =   0;
% Synthesis & Degradation
sele(is)       =   1;
sele = logical(sele);
```

```
disp('Choose degradation data');
[t_deg, Y_deg, sd_deg] = loadData();
disp('Choose constitutive internalization data');
[t_cint, Y_cint, sd_cint] = loadData();
disp('Choose agonist treatment data');
[t_ag, Y_ag, sd_ag] = loadData();
disp('Choose inverse agonist treatment data');
[t_inv, Y_inv, sd_inv] = loadData();

re = input('How many start points?');
k0s = lhsdesign(re, sum(sele)) - 0.5;
n_iter = input('How many iterations?');
trajK = [];
trajCurve1 = [];
trajCurve2 = [];
trajLH = [];
for i = 1 : re
    fprintf('\nStarting Point #%d\n', i)
    par = zeros(1, n_params2);
    par(sele) = k0s(i, :);
    par = denorm(par, rangs, scale);
    [ trajK_0, trajLH_0 ] =...
        MCMC_2lig( par, t_deg, t_ag, t_inv, ...
        Y_deg, Y_cint, Y_ag, Y_inv, sd_deg, sd_cint, sd_ag, sd_inv, ...
        @(k, r)stepdenorm( k, r, rangs, scale, sele ), n_iter);
    n_burn = ceil(0.2 * n_iter);
    trajK = [trajK, trajK_0(:, n_burn : end)];
    trajLH = [trajLH, trajLH_0(n_burn : end)];
end
x = num2str(rand());
save(['MCMC_2lig_results_', x, '.mat'], 'trajK', 'trajLH')
```

The Metropolis-Hastings algorithm is implemented as function `MCMC_2lig`:

```
function [ trajK, trajLH ]...
    = MCMC_2lig( par0, time, time_ag, time_inv, ...
Y_deg, Y_cint, Y_ag, Y_inv, sd_deg, sd_cint, sd_ag, sd_inv, stepfunc,
n_iter)
% MCMC Simulation on Parameter Space
% trajK -- all sampled Ks; trajLH -- likelihood associated with sampled Ks
% par0 -- initial parameter values;
% time: time points for constitutive data;
% time_ag: time points for agonist treatment data;
% time_inv: time points for inverse agonist treatment data;
% Y_deg: means for degradation data;
% Y_cint: means for constitutive internalization data;
% Y_ag: means for agonist treatment data;
% Y_inv: means for inverse agonist treatment data;
% sd_deg: standard deviation for degradation data;
% sd_cint: standard deviation for constitutive internalization data;
% sd_ag: standard deviation for agonist treatment data;
% sd_inv: standard deviation for inverse agonist treatment data;
% step_func: a function that change the values for parameters;
```

```
% n_iter: total number of iterations;

global R Rs LR LRs Rp eeRp eeR reR
global ik1 iKact ik3 iKa ia ie ...
ikp ikint ikdp iktr ikrec ikre5 is iRt iL...
i2a i2e i2Ka

n_tot = numel(par0);

trajK = zeros(n_tot, n_iter);
trajLH = zeros(1, n_iter);

first = 1;
n_acc = 0;
all_par = par0;
for i = 1 : n_iter
    fprintf('\nIteration #%d\n', i)

    % Create parameter set for constitutive, agonist, and inverse agonit
    ag_par = all_par;
    inv_par = all_par;
    inv_par(ia) = inv_par(i2a);
    inv_par(ie) = inv_par(i2e);
    inv_par(iKa) = inv_par(i2Ka);
    const_par = all_par;
    const_par(iL) = 0;

    % Calculate initial concentration
    ini_conc = initConc(all_par);

    % Remove unlabeled species (for constitutive data)
    unlabeled = ini_conc([eeRp, eeR, reR]);
    ini_conc([eeRp, eeR, reR]) = [0, 0, 0];

    % Constitutive simulation
    const_par(iL) = 0;
    [~, x] = solveodes_nosynth(ini_conc, [0; time * 3600], const_par,
@ode15s);

    xtot = sum(x(:, [R, Rs, Rp, eeRp, eeR, reR]), 2);
    xsur = sum(x(:, [R, Rs, Rp]), 2);
    xtot = xtot / xtot(1) * 100;
    xsur = xsur / xsur(1) * 100;
    xtot = xtot(2:end);
    xsur = xsur(2:end);

    % Agonist treatment
    ini_conc([eeRp, eeR, reR]) = unlabeled;
    [~, x] = solveodes(ini_conc, [0; time_ag * 3600], ag_par, @ode15s);
    x_ag = sum(x(:, [R, Rs, LR, LRs, Rp]), 2);
    x_ag = x_ag / x_ag(1) * 100;
    x_ag = x_ag(2:end);

    % Inverse agonist treatment
```

```
    [~, x] = solveodes(ini_conc, [0; time_inv * 3600], inv_par, @ode15s);
    x_inv = sum(x(:, [R, Rs, LR, LRs, Rp]), 2);
    x_inv = x_inv / x_inv(1) * 100;
    x_inv = x_inv(2:end);

    X = [xtot; xsur];
    Y = [Y_deg; Y_cint];
    V = [sd_deg.^2; sd_cint.^2];
    if isequal(size(X), size(Y))
        loglh = loglikelihood(Y, X, V);
    else
        loglh = -1e300;
    end

    X = [x_ag; x_inv];
    Y = [Y_ag; Y_inv];
    V = [sd_ag.^2; sd_inv.^2];
    if isequal(size(X), size(Y))
        loglh = loglh + loglikelihood(Y, X, V);
    else
        loglh = loglh - 1e300;
    end

    fprintf('Likelihood = Exp(%d)\n', loglh)

    if first == 1
        lastLH = loglh;
        lastK = all_par;
        first = 0;
        fprintf('Likelihood = Exp(%d)\n', loglh)
    else
        reP = exp(loglh - lastLH);
        fprintf('reP = %d\n', reP)
        r = rand();
        if r <= min([1, reP])
            % Accept
            lastLH = loglh;
            lastK = all_par;
            n_acc = n_acc + 1;
        else
            % Reject
            all_par = lastK;
            loglh = lastLH;
        end
        fprintf('Likelihood = Exp(%d)\n', loglh)
        fprintf('Accept Rate = %d\n', n_acc/i)
    end
    trajK(:, i) = all_par;
    trajLH(1, i) = loglh;

    % sample next parameters
    step = 0.08;
    r = 2 * step * rand(n_tot, 1) - step;
    all_par = stepfunc(all_par, r);
end
```

```
end

function [ P ] = likelihood( y, M, var )
%LIKELIHOOD Calculate the likelihood function
%   P -- likelihood
%   y -- prediction values;
%   M -- means of data; var -- variance of data
    p = exp(-0.5*(y-M).^2./var);
    P = prod(p);
end

function [ logP ] = loglikelihood( y, M, var )
%LOGLIKELIHOOD Calculate the logarithm of likelihood function
%   logP -- log likelihood
%   y -- prediction values;
%   M -- means of data; var -- variance of data
    logp = -0.5*(y-M).^2./var;
    logP = sum(logp);
end
```

Where the function `stepfunc` for perturbing the parameter vector is implemented as:

```
function [ y ] = stepdenorm( x, r, ranges, scale, sele )
%STEPDENORM perturb and denormalize the parameter space
%   y -- perturbed parameter vector
%   x -- original parameter vector
%   r -- step
%   ranges -- the range for parameters
%   scale -- 0 for log space, 1 for linear space
%   sele -- selected parameters

y = x;
for i = 1 : numel(x)
    if sele(i) ~= 0
        x1 = ranges(i, 1);
        x2 = ranges(i, 2);
        if scale(i) == 0
            y(i) = x(i) * (x2 / x1) ^ r(i);
            if y(i) > x2
                y(i) = x1/x2 * y(i);
            elseif y(i) < x1
                y(i) = x2/x1 * y(i);
            end
        else
            y(i) = x(i) + (x2 - x1) * r(i);
            if y(i) > x2
                y(i) = x1 + y(i) - x2;
            elseif y(i) < x1
                y(i) = x2 - (x1 - y(i));
            end
        end
```

```
    end
end

end
```

The calculation of SSE based on Eq.2.6.9:

```
function [ sse ] = calcSSE(  Ymean, Ysig, m, tY, X, tX  )
%CALCSSE calculate Sum of Squared Error for Prediction
%   Ymean -- data mean
%   Ysig -- data variance
%   m -- number of parallel experiments
%   tY -- time points for data
%   X -- simulation results
%   tX -- time points for simulation results

% Find the closest points for Y
I = ones(size(tY));
for i = 1 : numel(tY)
    least_d = abs(tY(i) - tX(1));
    for j = 2 : numel(tX)
        d = abs(tY(i) - tX(j));
        if d < least_d
            I(i) = j;
            least_d = d;
        else
            break;
        end
    end
end
X = X(I);

sse = (m - 1) * sum(Ysig .^ 2) + m * sum(Ymean .^ 2)...
    - m * sum(2 * Ymean .* X - X .^ 2);
end
```

The calculation of likelihood term for computing BIC based on Eq.2.6.11 and Eq.2.6.12:

```
function [ lh ] = calcLH(  Ymean, Ysig, m, tY, X, tX  )
%CALCSSE calculate the maximum likelihood
%   Ymean -- data mean
%   Ysig -- data variance
%   m -- number of parallel experiments
%   tY -- time points for data
%   X -- simulation results
%   tX -- time points for simulation results
```

```
% Find the closest points for Y
I = ones(size(tY));
for i = 1 : numel(tY)
    least_d = abs(tY(i) - tX(1));
    for j = 2 : numel(tX)
        d = abs(tY(i) - tX(j));
        if d < least_d
            I(i) = j;
            least_d = d;
        else
            break;
        end
    end
end
X = X(I);

lh = prod(1./sqrt(2 * pi * Ysig .^ 2)) * ...
    exp(-sum(sum( ((m - 1) * Ysig .^ 2 + m * Ymean .^ 2 ...
    - 2 * m * X .* Ymean + m * X .^ 2) ...
    ./ (2 * Ysig .^ 2) )));
end
```

The script that plot all the fitting results is coded in **plotmc4.m**:

```
clear
Initialize();
global R Rs LR LRs Rp eeRp eeR reR n_species names
global ik1 iKact ia iKa iL ie...
       ikp ikint ikdp iktr ikrec ikre5 is iRt knames ...
       i2a i2e i2Ka n_params2 knames2

files = dir(fullfile(pwd, 'Data'));
filemat.name = '';
filemat.type = '';
o = 0;
for i = 1 : numel(files)
    [~, filename, filetype] = fileparts(files(i).name);
    if (strcmp(filetype, '.mat'))
        newfile.name = filename;
        newfile.type = filetype;
        if (o == 0)
            filemat = newfile;
        else
            filemat = cat(2, filemat, newfile);
        end
        o = o + 1;
        prompt = strcat('    ', num2str(o), '. ', filename);
        fprintf('%s\n', prompt);
```

```
    end
end
re = input('Which file you want to analyze?');
load(strcat('Data\', filemat(re).name, filemat(re).type),...
    'trajK', 'trajLH');

disp('Choose degradation data.')
[~, Y_deg, sd_deg] = loadData();
disp('Choose constitutive internalization data.')
[time, Y_cint, sd_cint] = loadData();
disp('Choose agonist treatment data.')
[t_ag, Y_ag, sd_ag] = loadData();
disp('Choose inverse agonist treatment data.')
[t_inv, Y_inv, sd_inv] = loadData();

% some data transformation
for i = 1 : numel(trajLH)
    if(trajLH(i)<0)
        trajLH = exp(trajLH);
        break;
    end
end

% Find Best and Mean
[bestLH, I] = max(trajLH);
bestK = trajK(:, I);
meanK = 10.^(mean(log10(trajK), 2));

fprintf('\nLikelihood = %d\n', bestLH)
disp('Best Ks:')
for i = 1 : numel(bestK)
    fprintf('%s: %d\n', knames2{i}, bestK(i))
end
disp('Mean Ks:')
for i = 1 : numel(meanK)
    fprintf('%s: %d\n', knames2{i}, meanK(i))
end

%% Create parameter sets for 3 conditions
bestK_const = bestK;
bestK_const(iL) = 0;
bestK_ag = bestK;
bestK_inv = bestK;
bestK_inv(ia) = bestK_inv(i2a);
bestK_inv(ie) = bestK_inv(i2e);
bestK_inv(iKa) = bestK_inv(i2Ka);

%% Constitutive Dynamics

% Calculate initial concentration
ini_conc = initConc(bestK);
% Remove unlabeled species
ini_conc([eeRp, eeR, reR]) = [0, 0, 0];
```

```
[t, x] = solveodes_nosynth(ini_conc, [0, time(end) * 3600], bestK_const,
@ode15s);

xtot = sum(x(:, [R, Rs, Rp, eeRp, eeR, reR]), 2);
xsur = sum(x(:, [R, Rs, Rp]), 2);
xtot = xtot / xtot(1) * 100;
xsur = xsur / xsur(1) * 100;

figure()
hold on
errorbar(time, Y_deg, sd_deg, 'rx')
errorbar(time, Y_cint, sd_cint, 'rs')
thour = t / 3600;
plot(thour, xtot)
plot(thour, xsur, 'k')
xlabel('Time (hrs.)')
ylabel('% Starting Surface Receptor')
legend('Experiment: Degradation', 'Experiment: Internalization',...
    'Model: Degradation', 'Model: Internalization')
% Calculate Goodness-of-Fit Criteria
sse1 = calcSSE(Y_deg, sd_deg, 3, time, xtot, thour);
sse2 = calcSSE(Y_cint, sd_cint, 3, time, xsur, thour);
txt1 = ['SSE_1: ', num2str(round(sse1, 2))];
txt2 = ['SSE_2: ', num2str(round(sse2, 2))];
text(1, 50, txt1);
text(1, 40, txt2);
lh1 = calcLH(Y_deg, sd_deg, 3, time, xtot, thour);
bic1 = - 2 * log(lh1) + 8 * log(3 * 6);
lh2 = calcLH(Y_cint, sd_cint, 3, time, xsur, thour);
bic2 = - 2 * log(lh2) + 8 * log(3 * 6);
txt1 = ['BIC_1: ', num2str(round(bic1, 2))];
txt2 = ['BIC_2: ', num2str(round(bic2, 2))];
text(1, 45, txt1);
text(1, 35, txt2);
hold off

figure()
hold on
plot(thour, x)
xlabel('Time (hrs.)')
ylabel('Number of Molecules')
legend(names)
hold off

%% Ligand Treatment
% Calculate initial concentration
ini_conc = initConc(bestK);

% Agonist treatment
[t, x] = solveodes(ini_conc, [0, t_ag(end) * 3600], bestK_ag, @ode15s);
% Inverse agonist treatment
[t2, x2] = solveodes(ini_conc, [0, t_inv(end) * 3600], bestK_inv, @ode15s);

x_ag = sum(x(:, [R, Rs, LR, LRs, Rp]), 2);
x_ag = x_ag / x_ag(1) * 100;
```

```
x_inv = sum(x2(:, [R, Rs, LR, LRs, Rp]), 2);
x_inv = x_inv / x_inv(1) * 100;

figure()
% Agonist
subplot(121)
hold on
errorbar(t_ag, Y_ag, sd_ag, 'rx')
plot(t / 3600, x_ag)
xlabel('Time (hrs.)')
ylabel('% Starting Surface Receptor')
legend('Experiment: Agonist', 'Model best fit')
hold off
% Calculate Goodness-of-Fit Criteria
sse = calcSSE(Y_ag, sd_ag, 3, t_ag, x_ag, t / 3600);
txt = ['SSE: ', num2str(round(sse, 2))];
text(1.6, 85, txt);
lh = calcLH(Y_ag, sd_ag, 3, t_ag, x_ag, t / 3600);
bic = - 2 * log(lh) + 8 * log(3 * 6);
txt = ['BIC: ', num2str(round(bic, 2))];
text(1.6, 80, txt);

% Inverse agonist
subplot(122)
hold on
errorbar(t_inv, Y_inv, sd_inv, 'rx')
plot(t2 / 3600, x_inv)
xlabel('Time (hrs.)')
ylabel('% Starting Surface Receptor')
legend('Experiment: Inverse agonist', 'Model best fit')
hold off
% Calculate Goodness-of-Fit Criteria
sse = calcSSE(Y_inv, sd_inv, 3, t_inv, x_inv, t2 / 3600);
txt = ['SSE: ', num2str(round(sse, 2))];
text(8, 100, txt);
lh = calcLH(Y_inv, sd_inv, 3, t_inv, x_inv, t2 / 3600);
bic = - 2 * log(lh) + 8 * log(3 * 6);
txt = ['BIC: ', num2str(round(bic, 2))];
text(8, 80, txt);
hold off

figure()
hold on
plot(t / 3600, sum(x(:, [R, LR]), 2))
xlabel('Time (hrs.)')
ylabel('Number of Molecules')
%legend(names)
hold off

%% Distributions
K_names = {'R_t', 'Kact', 'kp', 'kint', 'kdp', 'ktr', 'krec', 's', 'a',
'2a', 'e', '2e'};
% Calculate the layout
ntot = numel(K_names);
m = ceil(ntot / 4);
n = min(ntot, 4);
```

```
figure()
for i = 1 : ntot
    subplot(m, n, i)
    par_idx = findcell(knames2, K_names{i});
    [trajKi, I] = sort(trajK(par_idx,:));
    trajLHi = trajLH(I);
    %semilogx(trajKi(trajLHi > 0.9), trajLHi(trajLHi > 0.9))
    semilogx(trajKi, trajLHi)
    xlabel(K_names(i))
    ylabel('Likelihood')
end

figure()
for i = 1 : ntot
    subplot(m, n, i)
    hold on
    par_idx = findcell(knames2, K_names{i});
    [nbins, xout] = hist(log10(trajK(par_idx,:)),60);
    bar(xout,nbins)
    xlabel(sprintf('log(%s)', K_names{i}))
    ylabel('Number')
    fprintf('%s mean: %d\n',K_names{i}, meanK(par_idx))
    % mean indicator
    p1 = ...
        plot([log10(meanK(par_idx)),log10(meanK(par_idx))],...
        [0, max(nbins)*1.1], '--', 'color',[0 0.5 0]);
    % best indicator
    p2 = ...
        plot([log10(bestK(par_idx)),log10(bestK(par_idx))],...
        [0, max(nbins)*1.1], 'r');
    legend([p1, p2], {'Mean', 'Best'})
    ylim([0, max(nbins)*1.1])
    hold off
end

%correlation plots
K_names = {'R_t', 'kint', 'krec'};
figure()
k = 0;
for i = 1 : 3
    for j = 1 : 3
        if (j > i)
        k = k + 1;
        subplot(1, nchoosek(numel(K_names), 2), k)
        par_idx1 = findcell(knames, K_names{i});
        par_idx2 = findcell(knames, K_names{j});
        K1 = log10(trajK(par_idx1,:));
        K2 = log10(trajK(par_idx2,:));
        scattercloud(K1, K2)
        xlabel(K_names{i})
        ylabel(K_names{j})
        end
    end
end
```

The codes for fitting and plotting for constitutive data are not shown, but they are simply a shortened version of above codes as they do not include ligand treatment data.

BIBLIOGRAPHY

1. Tuteja, N. Signaling through G protein coupled receptors. *Plant Signal. Behav.* **4,** 942–7 (2009).

2. Qin, K., Dong, C., Wu, G. & Lambert, N. A. Inactive-state preassembly of G(q)-coupled receptors and G(q) heterotrimers. *Nat. Chem. Biol.* **7,** 740–7 (2011).

3. Kenakin, T. The classification of seven transmembrane receptors in recombinant expression systems. *Pharmacol. Rev.* **48,** 413–463 (1996).

4. Zhou, Y.-Y. *et al.* Spontaneous activation of β2- but not β1-adrenoceptors expressed in cardiac myocytes from β1β2 double knockout mice. *Mol. Pharmacol.* **58,** 887–894 (2000).

5. Mancini, I. *et al.* Constitutive activity of cannabinoid-2 (CB 2) receptors plays an essential role in the protean agonism of (+)AM1241 and L768242. *Br. J. Pharmacol.* **158,** 382–391 (2009).

6. Milligan, G. Constitutive activity and inverse agonists of G protein-coupled receptors: a current perspective. *Mol. Pharmacol.* **64,** 1271–1276 (2003).

7. Oldham, W. M. & Hamm, H. E. Heterotrimeric G protein activation by G-protein-coupled receptors. *Nat. Rev. Mol. Cell Biol.* **9,** 60–71 (2008).

8. Park DT; Palczewski, K., P. L. Activation of G protein-coupled receptors: beyond two-state models and tertiary conformational changes. *Annu Rev Pharmacol Toxicol.* **48,** 107–141 (2008).

9. Park, P. S.-H. Ensemble of G protein-coupled receptor active states. *Curr. Med. Chem.* **19,** 1146–54 (2012).

10. DeWire, S. M., Ahn, S., Lefkowitz, R. J. & Shenoy, S. K. β-Arrestins and Cell Signaling.

Annu. Rev. Physiol. **69,** 483–510 (2007).

11. Perez, D. M. & Karnik, S. S. Multiple signaling states of G-protein-coupled receptors. *Pharmacol. Rev.* **57,** 147–61 (2005).

12. Bünemann, M., Frank, M. & Lohse, M. J. Gi protein activation in intact cells involves subunit rearrangement rather than dissociation. *Proc. Natl. Acad. Sci. U. S. A.* **100,** 16077–16082 (2003).

13. Levitzki, A. Regulation of adenylate cyclase by hormones and G-proteins. *FEBS Lett.* **211,** 113–118 (1987).

14. Millan, M. J., Marin, P., Bockaert, J. & Mannoury la Cour, C. Signaling at G-protein-coupled serotonin receptors: recent advances and future research directions. *Trends in Pharmacological Sciences* **29,** 454–464 (2008).

15. Hill, S. J. *et al.* International Union of Pharmacology. XIII. Classification of Histamine Receptors. *Pharmacol. Rev.* **49,** 253–278 (1997).

16. Beaulieu, J.-M. & Gainetdinov, R. R. The physiology, signaling, and pharmacology of dopamine receptors. *Pharmacol. Rev.* **63,** 182–217 (2011).

17. Turu, G. & Hunyady, L. Signal transduction of the CB1 cannabinoid receptor. *Journal of Molecular Endocrinology* **44,** 75–85 (2010).

18. Ofek, O. *et al.* CB2 cannabinoid receptor targets mitogenic Gi protein-cyclin D1 axis in osteoblasts. *J. Bone Miner. Res.* **26,** 308–316 (2011).

19. Connor, M. & Christie, M. D. Opioid receptor signalling mechanisms. *Clin Exp Pharmacol Physiol* **26,** 493–499 (1999).

20. Haga, T. Molecular properties of muscarinic acetylcholine receptors. *Proc. Jpn. Acad. Ser. B. Phys. Biol. Sci.* **89,** 226–56 (2013).

21. Busillo, J. M. & Benovic, J. L. Regulation of CXCR4 signaling. *Biochimica et Biophysica Acta - Biomembranes* **1768,** 952–963 (2007).

22. Daaka, Y., Luttrell, L. M. & Lefkowitz, R. J. Switching of the coupling of the beta2-adrenergic receptor to different G proteins by protein kinase A. *Nature* **390,** 88–91 (1997).

23. Megson, a C., Walker, E. M. & Hill, S. J. Role of protein kinase Calpha in signaling from the histamine H(1) receptor to the nucleus. *Mol. Pharmacol.* **59,** 1012–21 (2001).

24. Chen, Z. & Minneman, K. P. Recent progress in alpha1-adrenergic receptor research. *Acta Pharmacol. Sin.* **26,** 1281–1287 (2005).

25. Wang, D. *et al.* G proteins G12 and G13 control the dynamic turnover of growth factor-induced dorsal ruffles. *J. Biol. Chem.* **281,** 32660–32667 (2006).

26. Johnson, D. A., Akamine, P., Radzio-Andzelm, E., Madhusudan, M. & Taylor, S. S. Dynamics of cAMP-dependent protein kinase. *Chem. Rev.* **101,** 2243–2270 (2001).

27. Montminy, M. R. & Bilezikjian, L. M. Binding of a nuclear protein to the cyclic-AMP response element of the somatostatin gene. *Nature* **328,** 175–178 (1987).

28. Sánchez, M. G., Ruiz-Llorente, L., Sánchez, A. M. & Díaz-Laviada, I. Activation of phosphoinositide 3-kinase/PKB pathway by CB1 and CB2 cannabinoid receptors expressed in prostate PC-3 cells. Involvement in Raf-1 stimulation and NGF induction. *Cell. Signal.* **15,** 851–859 (2003).

29. Sugiura, T. *et al.* CARBOHYDRATES , LIPIDS , AND OTHER NATURAL PRODUCTS : Evidence That 2-Arachidonoylglycerol but Not N -Palmitoylethanolamine or Anandamide Is the Physiological Ligand for the Cannabinoid CB2 Receptor : COMPARISON OF THE AGONISTIC ACTIVITIES OF VARIOUS CANN. *J. Biol. Chem.* **275,** 605–12 (2000).

30. Shoemaker, J. L., Joseph, B. K., Ruckle, M. B., Mayeux, P. R. & Prather, P. L. The endocannabinoid noladin ether acts as a full agonist at human CB2 cannabinoid receptors. *J. Pharmacol. Exp. Ther.* **314,** 868–875 (2005).

31. Zamah, M. A., Delahunty, M., Luttrell, L. M. & Lefkowitz, R. J. Protein kinase A-mediated phosphorylation of the β2-adrenergic receptor regulates its coupling to Gs and Gi: Demonstration in a reconstituted system. *J. Biol. Chem.* **277,** 31249–31256 (2002).

32. Rapacciuolo, A. Protein Kinase A and G Protein-coupled Receptor Kinase Phosphorylation Mediates beta-1 Adrenergic Receptor Endocytosis through Different Pathways. *J. Biol. Chem.* **278,** 35403–35411 (2003).

33. Taussig, R., Iñiguez-Lluhi, J. a & Gilman, a G. Inhibition of adenylyl cyclase by Gi alpha. *Science* **261,** 218–221 (1993).

34. Pomerening, J. R. Uncovering mechanisms of bistability in biological systems. *Curr. Opin. Biotechnol.* **19,** 381–388 (2008).

35. Bouaboula, M., Dussossoy, D. & Casellas, P. Regulation of Peripheral Cannabinoid Receptor CB2 Phosphorylation by the Inverse Agonist SR 144528. *Biochemistry* **274,** 20397–20405 (1999).

36. Goodman, O. B. *et al.* Beta-arrestin acts as a clathrin adaptor in endocytosis of the beta2-adrenergic receptor. *Nature* **383,** 447–450 (1996).

37. Ribas, C. *et al.* The G protein-coupled receptor kinase (GRK) interactome: Role of GRKs in GPCR regulation and signaling. *Biochim. Biophys. Acta - Biomembr.* **1768,** 913–922 (2007).

38. Jovic, M., Sharma, M., Rahajeng, J. & Caplan, S. The early endosome: A busy sorting station for proteins at the crossroads. *Histol. Histopathol.* **25,** 99–112 (2010).

39. Grimsey, N. L., Goodfellow, C. E., Dragunow, M. & Glass, M. Cannabinoid receptor 2 undergoes Rab5-mediated internalization and recycles via a Rab11-dependent pathway. *Biochim. Biophys. Acta - Mol. Cell Res.* **1813,** 1554–1560 (2011).

40. Michaelis, L., Menten, M. L., Goody, R. S. & Johnson, K. A. Die Kinetik der Invertinwirkung/ The kinetics of invertase action. *Biochemistry* **49,** 333–369 (1913).

41. Resat, H., Petzold, L. & Pettigrew, M. F. Kinetic modeling of biological systems. *Methods Mol. Biol.* **541,** 311–335 (2009).

42. Black, C. A. Delayed type hypersensitivity: current theories with an historic perspective. *Dermatology online journal [electronic resource]* **5,** 7 (1999).

43. Shoemaker, P. A. Neural bistability and amplification mediated by NMDA receptors: Analysis of stationary equations. *Neurocomputing* **74,** 3058–3071 (2011).

44. Bagci, E. Z., Vodovotz, Y., Billiar, T. R., Ermentrout, G. B. & Bahar, I. Bistability in apoptosis: roles of bax, bcl-2, and mitochondrial permeability transition pores. *Biophys. J.*

90, 1546–59 (2006).

45. Wagner, J. & Stolovitzky, G. Stability and time-delay modeling of negative feedback loops. *Proc. IEEE* **96,** 1398–1410 (2008).

46. Northrop, D. B. Steady-state analysis of kinetic isotope effects in enzymic reactions. *Biochemistry* **14,** 2644–2651 (1975).

47. Voit, E. O., Martens, H. A. & Omholt, S. W. 150 Years of the Mass Action Law. *PLoS Comput. Biol.* **11,** (2015).

48. Liu, B., Bhatt, D., Oltvai, Z. N., Greenberger, J. S. & Bahar, I. Significance of p53 dynamics in regulating apoptosis in response to ionizing radiation, and polypharmacological strategies. *Sci. Rep.* **4,** 6245 (2014).

49. Bondarenko, V. E. A compartmentalized mathematical model of the β1-adrenergic signaling system in mouse ventricular myocytes. *PLoS One* **9,** (2014).

50. Mayawala, K., Vlachos, D. G. & Edwards, J. S. Spatial modeling of dimerization reaction dynamics in the plasma membrane: Monte Carlo vs. continuum differential equations. *Biophys. Chem.* **121,** 194–208 (2006).

51. Andrews, S. S., Addy, N. J., Brent, R. & Arkin, A. P. Detailed simulations of cell biology with Smoldyn 2.1. *PLoS Comput. Biol.* **6,** (2010).

52. Teusink, B. *et al.* Can yeast glycolysis be understood terms of vitro kinetics of the constituent enzymes? Testing biochemistry. *Eur. J. Biochem.* **267,** 5313–5329 (2000).

53. Arkin, a, Ross, J. & McAdams, H. H. Stochastic kinetic analysis of developmental pathway bifurcation in phage lambda-infected Escherichia coli cells. *Genetics* **149,** 1633–1648 (1998).

54. Linderman, J. J. Modeling of G-protein-coupled receptor signaling pathways. *J. Biol. Chem.* **284,** 5427–5431 (2009).

55. Hansson, E. K. *et al.* PKPD Modeling of VEGF, sVEGFR-2, sVEGFR-3, and sKIT as Predictors of Tumor Dynamics and Overall Survival Following Sunitinib Treatment in GIST. *CPT pharmacometrics Syst. Pharmacol.* **2,** e84 (2013).

56. Koch, G., Krzyzanski, W., Pérez-Ruixo, J. J. & Schropp, J. Modeling of delays in PKPD: Classical approaches and a tutorial for delay differential equations. *J. Pharmacokinet. Pharmacodyn.* **41,** 291–318 (2014).

57. Wurch, T. & Pauwels, P. J. Analytical pharmacology of G protein-coupled receptors by stoichiometric expression of the receptor and G(alpha) protein subunits. *J. Pharmacol. Toxicol. Methods* **45,** 3–16 (2001).

58. Kenakin, T. & Christopoulos, A. Analytical pharmacology: The impact of numbers on pharmacology. *Trends in Pharmacological Sciences* **32,** 189–196 (2011).

59. Cao, Y., Gillespie, D. T. & Petzold, L. R. Multiscale stochastic simulation algorithm with stochastic partial equilibrium assumption for chemically reacting systems. *J. Comput. Phys.* **206,** 395–411 (2005).

60. Meier-Schellersheim, M., Fraser, I. & Klauschen, F. Multi-scale modeling in cell biology. *Wiley Interdiscip. Rev. Syst. Biol. Med.* **1,** 4–14 (2009).

61. Aj, C. *The mode of action of drugs on cells*. (Williams & Wilkins, 1933). doi:10.1038/132695d0

62. ARIENS, E. J. Affinity and intrinsic activity in the theory of competitive inhibition. I. Problems and theory. *Arch. Int. Pharmacodyn. thérapie* **99,** 32–49 (1954).

63. Weiss, J. N. The Hill equation revisited: uses and misuses. *FASEB J.* **11,** 835–841 (1997).

64. Alexander, S., Mathie, A. & Peters, J. G Protein-Coupled Receptors. *Br. J. Pharmacol.* **164,** S5–S113 (2011).

65. Kenakin, T. Efficacy at G-protein-coupled receptors. *Nat. Rev. Drug Discov.* **1,** 103–110 (2002).

66. Kinzer-Ursem, T. L. & Linderman, J. J. Both ligand- and cell-specific parameters control ligand agonism in a kinetic model of G protein-coupled receptor signaling. *PLoS Comput. Biol.* **3,** 0084–0094 (2007).

67. Weiss, J. M., Morgan, P. H., Lutz, M. W. & Kenakin, T. P. The cubic ternary complex receptor-occupancy model. I. model description. *J. Theor. Biol.* **178,** 151–167 (1996).

68. Weiss, J. M., Morgan, P. H., Lutz, Mi. W. & Kenakin, T. P. The Cubic Ternary Complex Receptor–Occupancy Model II. Understanding Apparent Affinity. *J. Theor. Biol.* **178,** 169–182 (1996).

69. Drive, F. M. The Cubic Ternary Complex Receptor-Occupancy Model III. Resurrecting Efficacy. *J. Theor. Biol.* **181,** 381–397 (1996).

70. Vayttaden, S. J. *et al.* Quantitative modeling of GRK-mediated beta2AR regulation. *PLoS Comput. Biol.* **6,** e1000647 (2010).

71. Tan, W. H., Popel, A. S. & Mac Gabhann, F. Computational model of VEGFR2 pathway to ERK activation and modulation through receptor trafficking. *Cell. Signal.* **25,** 2496–2510 (2013).

72. Coggins, N. L. *et al.* CXCR7 controls competition for recruitment of beta-arrestin 2 in cells expressing both CXCR4 and CXCR7. *PLoS One* **9,** 1–14 (2014).

73. Carrier, E. J. *et al.* Cultured rat microglial cells synthesize the endocannabinoid 2-arachidonylglycerol, which increases proliferation via a CB2 receptor-dependent mechanism. *Mol. Pharmacol.* **65,** 999–1007 (2004).

74. Butcher, J. C. *Numerical Methods for Ordinary Differential Equations*. *Methods* (2008). doi:10.1002/9780470753767

75. Lasagni, F. M. Canonical Runge-Kutta methods. *ZAMP Zeitschrift f??r Angew. Math. und Phys.* **39,** 952–953 (1988).

76. Bolognini, D., Cascio, M. G., Parolaro, D. & Pertwee, R. G. AM630 behaves as a protean ligand at the human cannabinoid CB 2 receptor. *Br. J. Pharmacol.* **165,** 2561–2574 (2012).

77. Olsson, D. M. & Nelson, L. S. The Nelder-Mead Simplex Procedure for Function Minimization. *Technometrics* **17,** 45–51 (1975).

78. Luersen, M. A. & Le Riche, R. Globalized nelder-mead method for engineering optimization. in *Computers and Structures* **82,** 2251–2260 (2004).

79. Rizk, M. L. & Liao, J. C. Ensemble modeling and related mathematical modeling of metabolic networks. *J. Taiwan Inst. Chem. Eng.* **40,** 595–601 (2009).

80. Kuepfer, L., Peter, M., Sauer, U. & Stelling, J. Ensemble modeling for analysis of cell signaling dynamics. *Nat. Biotechnol.* **25,** 1001–1006 (2007).

81. Metropolis, N., Rosenbluth, A. W., Rosenbluth, M. N., Teller, A. H. & Teller, E. Equation of State Calculations by Fast Computing Machines. *J. Chem. Phys.* **21,** 1087–1092 (1953).

82. Chib, S. & Greenberg, E. Understanding the Metropolis-Hastings Algorithm. *The American Statistician* **49,** 327 (1995).

83. Swigon, D. Ensemble Modeling of Biological Systems. *Math. Life Sci.* 19–42 (2012).

84. Stein, M. Large Sample Properties of Simulations Using Latin Hypercube Sampling. *Technometrics* **29,** 143–151 (1987).

85. Rosner, B. *Fundamentals of Biostatistics*. (Brooks/Cole, 2011).

86. Resat, H., Ewald, J. A., Dixon, D. A. & Wiley, H. S. An integrated model of epidermal growth factor receptor trafficking and signal transduction. *Biophys. J.* **85,** 730–743 (2003).

87. Faeder, J. R. *et al.* Investigation of early events in FcεRI-mediated signaling using a detailed mathematical model. *J. Immunol.* **170,** 3769–3781 (2003).

88. Warne, T. *et al.* The structural basis for agonist and partial agonist action on a β(1)-adrenergic receptor. *Nature* **469,** 241–4 (2011).

89. Kenakin, T. Inverse, protean, and ligand-selective agonism: matters of receptor conformation. *FASEB J.* **15,** 598–611 (2001).

90. Ballmer-Hofer, K., Andersson, A. E., Ratcliffe, L. E. & Berger, P. Neuropilin-1 promotes VEGFR-2 trafficking through Rab11 vesicles thereby specifying signal output. *Blood* **118,** 816–826 (2011).

91. Gampel, A. *et al.* VEGF regulates the mobilization of VEGFR2/KDR from an intracellular endothelial storage compartment. *Blood* **108,** 2624–2631 (2006).

92. Nakayama, M. & Berger, P. Coordination of VEGF receptor trafficking and signaling by coreceptors. *Experimental Cell Research* **319,** 1340–1347 (2013).

93. Kleyer, J. *et al.* Cannabinoid receptor trafficking in peripheral cells is dynamically regulated

by a binary biochemical switch. *Biochem. Pharmacol.* **83,** 1393–1412 (2012).

94. Donzé, A., Clermont, G. & Langmead, C. J. Parameter synthesis in nonlinear dynamical systems: application to systems biology. *J. Comput. Biol.* **17,** 325–336 (2010).